Master's Thesis

Effect of Gd-alloyed Neutron Absorber on Thermal Performance of a Spent Fuel Cask

Hee-Jae Lee

Department of Nuclear Engineering

Graduate School of UNIST

2017

Effect of Gd-alloyed Neutron Absorber on Thermal Performance of a Spent Fuel Cask

Hee-Jae Lee

Department of Nuclear Engineering

Graduate School of UNIST

Effect of Gd-alloyed Neutron Absorber on Thermal Performance of a Spent Fuel Cask

A thesis
submitted to the Graduate School of UNIST
in partial fulfillment of the
requirements for the degree of
Master of Science

Hee-Jae Lee

07. 16. 2017

Approved by

Advisor
Prof. Sohn Dong-Seong

Effect of Gd-alloyed Neutron Absorber on Thermal Performance of a Spent Fuel Cask

Hee-Jae Lee

This certifies that the thesis of Hee-Jae Lee is approved.

07/16/2017

Signature

Dong-Seong Sohn

Signature

In Cheol Bang

Signature

Sung Yeol Choi

Abstract

A spent fuel cask must be designed to provide safety functions. In particular, in order to maintain the sub-criticality safety, different neutron absorbers have been used for the spent nuclear fuel management system. Although BORAL is the most used neutron absorber, several problems have been reported and it has some potential problems for long term storage of spent nuclear fuels. Recently, a Gd-alloyed duplex stainless steel demonstrated the possibility of fabrication and under development for an advanced neutron absorber and structural material as well. In this study, the effect of Gd alloyed neutron absorber on thermal performance of a spent fuel cask has been studied. The thermal properties of Gd-alloyed DSS was measured using the specimens provided by KITEC. The effect of Gd-alloyed duplex stainless steel adoption was analyzed for the reference casks, KSC-1 and KORAD-21. The analysis method was verified by comparing the analysis results with the reported values. Their system with Gd-alloyed DSS should remove decay heat with passive cooling. The KSC-1 and KORAD-21 casks were modeled with a 2D axis-symmetry condition and 3D symmetry condition, respectively, using ANSYS FLUENT v17.0. Based on the verified method, thermal performance of KORAD-21 which adopts Gd-alloyed DSS was analyzed. The maximum fuel cladding temperature with Gd-alloyed DSS exceeded allowable temperature of 400 ℃ and it could affect the fuel integrity. Therefore, basket wall thickness and disk thickness were optimized to enhance thermal performance. When the basket wall thickness was reduced, the gap between the basket surface and disk square holes was consequently increased. The increased gap enhanced the upward flow of helium and it improved the decay heat removal. Additionally, disk thickness was optimized to 60mm from 20mm. The increased heat-conducting surface enhanced the conduction heat transfer. As a result, UNIST-version design of the KORAD-21 cask was developed with the 5.0mm basket wall thickness and 60mm disk thickness. Thermal performance of UNIST design cask satisfied thermal requirements in normal operation.

Keywords: Gd-alloyed duplex stainless steel, thermal performance, spent fuel cask, thermal analysis

Contents

List of Figures

List of Table

Nomenclature

Variable	Description	Unit
β	The volumetric thermal expansion coefficient	K^{-1}
ρ	Density	$kg \cdot m^{-3}$
ρ_m	Measured density	$g \cdot cm^{-3}$
T	Temperature	K
T_i	Temperature of basket inner surface	K
T_o	Temperature of basket outer surface	K
T_{sur}	Temperature of cask surface	K
T_{amb}	Temperature of ambient temperature	K
T_{cal}	Calculated temperature	K
T_{rep}	Temperature in the report	K
M_w	The molecular weight	$g \cdot mol^{-1}$
R	The universal gas constant	$J \cdot K^{-1} \cdot mol^{-1}$
P_{op}	Operating pressure	Pa
g	Gravity	$m \cdot s^{-2}$
q	Heat flow rate	W
q''	Heat flux	$W \cdot m^{-2}$
A	The heat transferred area	m^2
k	Thermal conductivity	$W \cdot m^{-1} \cdot K^{-1}$
k_{eff}	The effective thermal conductivity of composite walls	$W \cdot m^{-1} \cdot K^{-1}$
k_{air}	Thermal conductivity of air	$W \cdot m^{-1} \cdot K^{-1}$
R_t	Total thermal resistance	$K \cdot W^{-1}$
R_x	Resistance of each component, x	$K \cdot W^{-1}$
C_p	Specific heat	$J \cdot g^{-1} \cdot K^{-1}$
α	Thermal diffusivity	$mm^2 \cdot s^{-1}$
m	Mass	kg
K_c	The Cowan correlation	-
Δt	Difference of temperatures at 5 half-times and 10 half-times	K
h	Heat convection coefficient	$W \cdot m^{-2} \cdot K^{-1}$
σ	Stefan-Boltzmann constant	$W \cdot m^{-2} \cdot K^{-4}$
Gr	Grashof number	-
Ra	Rayleigh number	-
Pr	Prantl number	-
Nu	Nusselt number	-
D	The characteristic diameter of cask	m
L	The characteristic length of cask	m
v	Kinematic viscosity	$m^2 \cdot s^{-1}$
θ	Temperature difference	-

Acknowledgements

In writing my thesis, I have contracted many debts. First of all, I should like to thank Prof. Sohn Dong-Seong for allowing me to continue my education at UNIST and than offering constant assistance. His guidance helped me in all the time of research of this thesis. I could not have imagined having a better advisor and mentor for my study. Besides, I would like to thank my thesis committee who have commented on this thesis: Prof. Bang In Cheol and Prof. Choi Sung Yeol for their encouragement.

Furthermore, I would like to thank my laboratory members: Mi Jin Kim, Gwan Yoon Jeong, Cheol Min Lee, Tae Won Cho and Ji Hyun Kim for stimulating discussion, and for all the fun we have had. Also, I thank my friends who have read and supported this thesis: Ha Ni Lee, Ji Soo Kim and Hye Jin Lee. I would like to record my gratitude to a number of individual who have given me help and encouragement.

Finally, I also want to take this opportunity to thank to my family, especially my parents, Nam Won Lee and Mi Young and to my partner, Daeil Lee. They have assisted me in innumerable ways, whatever I might say here cannot do full justice to the extent and the value of their contribution. This accomplishment would not have been possible without them. Thank you.

I. Introduction

1.1 Spent fuel cask

Spent nuclear fuel (SNF) is a type of nuclear fuel used in a nuclear reactor, that has undergone a fission chain reaction. After absorbing neutrons, the reaction produces minor actinides and fission products with a long half-life. According to the domestic standard fuel (42GWd/tU), the short half-life nuclides such as Sr-90, Y-90 and Cs-137 have a significant influence on decay heat generation [1]. Because of this, the SNF withdrawn from the nuclear reactor should undergo a cooling period. Currently, interim or long-term storage options for domestic SNFs have been considered with a dry storage system. After proper cooling period in the spent fuel pool, the SNF can be transferred to the dry storage cask. The dry storage cask differs from the wet storage system in that it uses gas or air as a coolant. In addition, the dry storage cask uses concrete or metal as a radiation–shielding material. The system must also be designed to remove a sufficient amount of emitted decay heat from the SNF without activation of the cooling systems. Transferring SNFs from wet to dry storage begins by placing the empty fuel canister into a transfer cask that provides radiation shielding. The transfer cask with the canister inside is lowered by crane into the spent fuel pool. SNFs then are placed in the fuel canister. After loading SNFs, the transfer cask is removed from the pool, and the water is drained out with vacuum drying. The canister loading SNFs is transferred to cask body [2].

The cask system primarily comprises of a cask body and a canister, which loads the SNF. The canister is a primary cylindrical pressure vessel made of stainless steel. The cask body and canister provide containment of radioactive materials with a cask lid, a canister lid, lid bolts and nuts. The structure of the cask body is composed of lead and a neutron–shielding material, which provides shielding of neutrons and gamma rays. Inside the canister, there are square boxes known as baskets. The baskets structurally support the SNF and the subcriticality with a neutron absorber during fuel loading and storage.

Depending on the cask body material, the cask system is classified as a concrete cask or a metal cask. The cask can also be classified according to its purpose of use. A cask used solely for transportation of the SNF is called as transportation cask. A storage cask aims to store the SNF in a dry system, and it can also be used for transportation if necessary. Recently, studies have been conducted on the use of a metal cask for the dual purpose of transportation and storage. The domestic spent fuel casks, such as KSC-1 and KSC-4, were developed by Korea Atomic Energy Research Institute (KAERI) in order to transport SNF for testing. Additionally, in 2002, a KN-12 cask was developed to transport 12 PWR spent fuel assemblies. This KN-21 cask is used inside the Kori nuclear power plant. Recently, a KORAD-21 that can contain 21 spent fuel assemblies was developed in 2016. Besides, the high-

capacity storage system which can load PWR 32 spent fuel assemblies are under development. Spent fuel inventory is in a trend toward higher capacities [3].

1.2 Neutron absorber

1.2.1 Existing neutron absorber

Neutron absorbing materials are used in order to maintain the sub-criticality condition of the SNF management system. It is fabricated using thermal neutron absorbing materials which have a high thermal neutron absorption cross-section, such as boron, gadolinium, and samarium. Boron has been used as a neutron–absorbing material that can be applied to spent fuel storage systems. In particular, boron-10 has an excellent thermal neutron–absorbing cross-section of 3800 barn. Neutron absorbers can be manufactured in various forms of alloy, compound, and composite material. This variety includes BORAFLEX, BORAL, boronated aluminum alloy, and boronated stainless steel alloy, with BORAL being the most used neutron absorber in SNF management. BORAL comes in a form in which boron carbide powder is dispersed in an aluminum-1100 matrix and covered with aluminum foil [4]. BORAL alone cannot be used as a structure material, but has been used in the form of composite structure as shown in Figure 2. Existing basket structure consists of three walls, such as inner stainless steel, BORAL, and outer stainless steel. BORAL adheres to four sides of the stainless steel structure, wrapped by a thin layer of stainless steel as a sheathing.

BORAL has been continuously installed in the basket of spent fuel cask and several issues on BORAL have been raised. First, the boron carbide particles with boron-10 can effectively absorb thermal neutrons, but at the same time can lead to the production of several transmutation species such as helium and lithium, according to the $B^{10}(n,\alpha)\,Li^{7}$. The helium bubbles may affect the neutron absorption behavior and the reduced thermal conductivity [5]. Secondly, the blister formation on the aluminum foil of BORAL was observed at the AECL Chalk River Laboratory in Canada [4]. Even after vacuum drying of the spent fuel cask, some water may continue to reside, and residual water is especially concerning for any aluminum component. Residual water can enter the BORAL through the exposed edges. During cask vacuum drying, the temperature rises to 400 ˚C and the escape path is blocked. Blisters can be formed along the aluminum foils. It can cause inward deformation of outer stainless steel sheathing reducing the free clearance of BORAL [2, 6]. Thirdly, residual water can cause corrosion of aluminum foil of BORAL by galvanic coupling between stainless steel and aluminum foil and subsequently hydrogen gas is generated [2, 7]. Formation of the hydrogen gas can cause a bulging of the outer stainless steel [8]. Moreover, it can create an explosion during the cask lid welding process [2].

1.2.2 Gd-alloyed duplex stainless steel

Many studies on the commercial neutron absorbing materials have been made on boron, but it is also known that Gd has the highest thermal neutron absorption cross-section among any stable nuclide: about 255,000 barns. In particular, that of $\mathbf{Gd^{157}}$ is approximately 66 times that of $\mathbf{B^{10}}$, as shown in Table 1. In addition, Gd isotopes remain as Gd after it absorbs neutron and also have good thermal neutron absorption ability. The relative abundance of $\mathbf{Gd^{155}}$and $\mathbf{Gd^{157}}$is 30.45 %, and does not require an enrichment process. Previous studies suggested that the criticality decreases as an increase of neutron absorbing material contents. Figure 4 shows that Gd exponentially decreases as Gd content increases. The B curve shows less steep slope than Gd curve. Gd addition shows stronger effect than B addition. The Gd experiences a higher performance compared to B at the same atomic contents [9, 10].

Duplex Stainless Steel (DSS) is a type of various stainless steels and has a combination of ferrite and austenite stainless steels. DSS offers good resistance to corrosion and stress corrosion cracking, and high mechanical strength [11]. In this regard, Gd containing DSS can be formed of only single wall and can serve dual roles as a structure material and a neutron absorber. The single wall structure has advantageous in that the problems coming from the composite wall structure does not occur such as corrosion and blisters. Moreover, $(\boldsymbol{n}, \boldsymbol{\alpha})$ reaction does not occur because it is based on Gd. Recently, a new Gd-alloyed duplex stainless steel was manufactured with 1wt.% Gd by melting, casting, and hot-rolling [11]. It was found that gadolinium with the main alloy elements are dispersed around the matrix, which means that neutron absorbing capability is also uniformly distributed [11]. Gd-alloyed DSS demonstrated enough the possibility of fabrication and development as a neutron absorbing structural material.

1.3 Thermal performance of a spent fuel cask

The structures and components of the spent fuel cask must be able to perform essential functions important to safety. The safety requirements for the transportation and storage casks have been presented [12-15]. The needs with regard to cask safety include criticality, safety, decay heat removal, radiation shielding, containment of radioactive materials and structural maintenance. Particularly, the decay heat generated from the SNFs must be sufficiently removed, with each component performing their safety functions. A dry storage cask is designed for about several decades of use. During the period, aging time will affect thermal integrity of the components in the system. Therefore, all components in the cask must be satisfied for thermal design criterion for use. The dry storage cask may be exposed to

low or high temperature conditions due to climate change. Moreover, moisture in the atmosphere and different climate change can affect the cask system. It is necessary to evaluate whether the cask can maintain thermal performance by passive cooling under several conditions and whether each component does not exceed the allowable temperature. In the case of spent fuel cladding, thermal creep is the dominant mechanism for cladding deformation and it can lead to gross rupture of the spent fuel cladding. In this regards, the allowable maximum temperature of 400 ℃ and 1% creep strain criterion were proposed by NRC to maintain integrity of spent fuel cladding in normal operation [16]. In the case of gamma shield, a high density material is likely to shield gamma ray, whereby gamma shielding material is composed of high number atoms, such as lead, carbon steel and concrete. The thermal criterion of the gamma shielding material can be based on the allowable temperature recommended by ASME so as to maintain its shielding ability. In contrast, a material consisting of low number atoms is suitable for absorbing thermal neutrons. The materials including hydrogen have been used as neutron shielding material. When the temperature of the neutron shielding material is changed drastically, a loss of hydrogen content is caused by a change in density, and the neutron shielding ability can be lowered [14]. In the case of NS-4-FR, which is a type of Resin as a neutron shielding material, it was observed that the material was degraded with decrease of its weight at high temperature [17]. For this reason, the safe operating temperature of the material was proposed to satisfy 150℃ or less. Furthermore, previous research has been conducted in order to predict the maximum fuel cladding temperature [18-22], and to confirm thermal safety of components in the cask using computer codes [23-26].

In this study, the Gd–alloyed DSS was considered as a new neutron absorber in the spent fuel cask. BORAL is manufactured based on an aluminum matrix and has good thermal conductivity of about 86 W/m· K, whereby it has been used in decay heat removal system. Since basket is directly and structurally connected to the stored SNFs, it can sufficiently influence the decay heat removal capability. In this regard, the purpose of this paper is to offer an effect of Gd–alloyed DSS on thermal performance of the spent fuel cask and to optimize cask design for application of Gd-alloyed DSS. ANSYS FLUENT v17.0 was used for a computational fluid dynamics (CFD) simulation. The reference casks used for the application were the KSC-1 and KORAD-21 casks. The following chapter will focus on the thermal analysis of these reference casks with Gd–alloyed DSS.

II. Analysis method and verification

2.1 Cask model

2.1.1 KSC-1

The KSC-1 cask was developed in 1985 for the transportation of a fuel assembly from the NPP to KAERI [27]. It has a history of carrying the SNFs multiple times since 1987. KSC-1 is a wet–type transportation cask, and is filled with water. The total weight of the KSC-1 cask is about 28 tons with a diameter of 1.11 m. The total length of the cask, to include the impact limiter, is 5.23 m [28]. Figure 6 below shows the design characteristics of the KSC-1 cask. Considering the computational time, a 2-D axisymmetric model was used for the thermal analysis of the KSC-1, as shown in Figure 7. It was based on the assumption that the KSC-1 cask is in the horizontal position. The gravity vector was applied to the y-axis as -9.81 m/s^2. It is assumed that there were 12 PWR fuel rods in the fuel region and that the heat is generated equally throughout the fuel volume. The fuel region was modeled using an effective radius that would give it the same volume as 12 fuel rods.

A fluid in the inner cavity experiences a natural convection flow induced by buoyancy due to the fluid density gradient ($\Delta\rho$) and the body force such as gravity (g) [29]. In addition, the density gradient ($\Delta\rho$) can be caused by the temperature gradient (ΔT) with decay heat and can be approximated with the temperature gradient (ΔT) and the volumetric thermal expansion coefficient (β). This approximation treats the density as a constant and solves as a function of temperature as follows[29] .

$$\beta \approx -\frac{1}{\rho}\frac{\Delta\rho}{\Delta T} = -\frac{1}{\rho}\frac{\rho_\infty - \rho}{T_\infty - T}$$

$$\rho_\infty - \rho \approx \rho\beta(T - T_\infty)$$

Using this approach, the density of water is specified a constant and the analysis can be gotten faster to convergence. In addition, a buoyancy-induced laminar flow model was applied to water flow.

2.1.2 KORAD-21

The KORAD-21 cask is a metal cask that has been developed recently by Korea Radioactive Waste Agency. It can load 21 fuel assemblies of WH or CE types, and is designed for dual purposes (storage and transportation). The cask body is made of carbon steel with a canister made of stainless steel. Within the canister are fuel assemblies, baskets, disks, rod supports, and fuel supports. Baskets containing SNFs are placed at regular intervals and are supported by disks. At the bottom of the SNFs, fuel supports hold up the fuel assemblies, which keep its bottom surfaces from making direct contact with the canister surface. These complex structures inside the canister are sealed primarily via a canister lid. A neutron–shielding shell, which is installed with heat transfer fins, surrounds the cask body. The cask body, containing the shell, has a height of 5.285 m and a diameter of 2.384 m.

The KORAD-21 cask was modeled using a three–dimensional and one–quarter axial symmetry condition as shown in Figure 9 and Figure 10. It was assumed to be under storage conditions with a vertical installation. The gravity vector was applied to the z–axis as -9.81 m/s^2. In regards to the fuel region, modeling explicitly all the individual structures of the fuel assemblies is difficult and time-consuming and requires extensive analysis. According to the general guidance on CFD analysis of the storage cask, the fuel assemblies can be simplified as a homogeneous region utilizing a porous media [15]. In order to simulate the convective heat transfer in the porous medium, flow resistance was applied using the pressure drop method [30]. In addition, thermal properties of the region for estimation of peck cladding temperature need to be determined. CFD simulations were additionally performed for WH17X17, WH16X16 and PLUS7. The calculated effective thermal conductivity values were applied to the aforementioned porous medium [31].

To simulate the natural convection of inner cavity helium, the incompressible ideal gas law was used to calculate the density (ρ) of helium. The incompressible ideal gas law applies in the case of a single-fluid problem with an operating pressure (P_{op}) in a closed cavity.

$$\rho = \frac{P_{op}}{\frac{R}{M_w}T}$$

2.2 Thermal property

2.2.1 KSC-1 components

The KSC-1 cask has three cylindrical shells and a cask body, which are manufactured using stainless steel. Inside the inner shell, an SNF is stored in the basket, and the inner cavity is filled with water for the cooling of decay heat. The intermediate shell contains lead used to shield gamma radiation emitted from the SNF. The outer shell includes water, air, and an ethylene-glycol mix. The mixture provides neutron shield. The materials of the KSC-1 components are described in Table 2.

2.2.2 KORAD-21 components

The KORAD-21 mainly consists of the canister, which stores spent fuel assemblies, cask body, which serve decay heat removal and radiation shielding. All components within the canister are formed of stainless steel including the canister. BORAL is used as a neutron absorber with basket structure. Table 3 describes the materials of the components.

2.2.3 Existing neutron absorber; BORAL case

The KORAD-21 cask adopts BORAL as a neutron absorber with the structure material formed of stainless steel. BORAL is attached to the inner stainless steel of 5.0mm. The total wall thickness of the conventional basket is 9.5mm including the outer stainless steel and BORAL. Modeling explicitly all the walls is difficult and time-consuming. Heat transfer rate in homogenized composite walls is related to a temperature difference and thermal conductivity. The basket model can be homogenized with a effective thermal conductivity. Heat transfer rate can be expressed using the thermal resistance concept of composite walls as shown below.

$$\mathrm{Q} = k_{\mathrm{eff}} \cdot A \frac{T_i - T_o}{L}$$

$$\mathrm{Q} = \frac{T_i - T_o}{R_t}$$

The effective thermal conductivity for the homogenized composite walls can be obtained using the thermal resistance for conduction.

$$\mathrm{k_{eff}} = \frac{L}{R_t \cdot A}$$

In the case of thickness direction, it is assumed that inner and outer surfaces of the basket are in an isothermal condition. The total thermal resistance for thickness direction is as follows.

$$R_t = \frac{1}{\frac{1}{R_1 + R_2} + \frac{1}{R_3} + \frac{1}{R_4 + R_5 + R_6} + \frac{1}{R_7} + \frac{1}{R_8 + R_9}}$$

In the case of parallel direction, it is assumed that the inner and outer surfaces of the basket are under adiabatic conditions. The total thermal resistance for parallel direction is as follows.

$$\mathrm{R_t} = \frac{R_1 \cdot R_2}{R_1 + R_2} + R_3 + \frac{R_4 \cdot R_5 \cdot R_6}{R_5 R_6 + R_4 R_6 + R_4 R_5} + R_7 + \frac{R_8 \cdot R_9}{R_8 + R_9}$$

2.2.4 Gd-alloyed duplex stainless steel

It is known that thermal conductivity of gadolinium has very low thermal conductivity among metallic compounds. In order for gadolinium to evaluate the influence on DSS, it is necessary to measure thermal properties of Gd-alloyed DSS. In this work, the thermophysical properties of Gd–alloyed DSS were measured using Laser Flash Analysis (LFA) and Differential Scanning Calorimeter (DSC) method. The specimens were prepared by KITECH and based on the manufacturing method and Gd contents.

The specimen thickness was measured 5 times for each specimen and the average value from that was used in density calculations. The calculated densities are shown in Table 5. The density of the commercial duplex stainless steel is known as about 7.8 g/cc. The specimens have similar values to that of commercial DSS and there is no clear trend with Gd contents. The results showed that the samples fabricated by hot rolling have a higher density than those fabricated by casting.

Specific heat is a thermodynamic quantity, which shows the extent of an increase in temperature by adding heat per unit mass. It can be obtained by using the relationship between the heat flow rate given to a sample and the temperature increase of the material. Differential scanning calorimeter (DSC) is the most widely used technique for measuring the specific heat of a material [32]. The specific heat results were measured from 50 ℃ to 400 ℃ using the DSC method, as shown in Table 6. The error of the DSC measurement was set at 5% and the results of the Gd–added samples were within the error range. Yet this did not show a trend relative to Gd contents. Therefore, the Gd addition of about 0.6-0.7 wt.% hardly affects the specific heat of DSS.

$$\mathrm{C_p} = \frac{\Delta Q}{m \cdot \Delta T}$$

Laser Flash Analysis (LFA) has been used for measuring thermal diffusivity. When the laser pulse or flash is irradiated in front of the specimen, the absorbed thermal energy is transferred to the back of the specimen. The temperature on the back surface becomes saturated as maximum temperature with the lapse of time. Using the temperature differences, thermal diffusivity can be obtained using the Cowan model [33].

$$\alpha = \alpha_{0.5} \cdot \frac{K_c}{0.13885}$$

$$\mathrm{K_c} = a + b(\Delta t) + \mathrm{c}(\Delta \mathrm{t})^2 + d(\Delta t)^3 + e(\Delta t)^4 + f(\Delta t)^5 + g(\Delta t)^6 + h(\Delta t)^7$$
$$\Delta \mathrm{t} = \text{Difference of temperatures between 5 Half} - \text{times and 10 Half} - \text{times}$$

The measured data, such as the density, specific heat, and thermal diffusivity, are correlated with one another, and are used for converting thermal conductivity. This method has been frequently used to obtain thermal conductivity as shown below. Thermal conductivity was calculated by multiplying the measured thermal diffusivity, density and specific heat. It is shown in Table 9.

$$\mathrm{k(T)} = \rho_{\mathrm{m}}(\mathrm{T}) \cdot \mathrm{C_p}(T) \cdot \alpha(T)$$

2.2.5 Thermal conductivities of neutron absorbers

Thermal conductivities (TCs) of an existing neutron absorber, composed of a composite structure with BORAL, was calculated using the thermal resistance model for thickness and parallel directions. Calculated results for each direction are shown in Figure 18. Since BORAL is based on the aluminum matrix, the existing neutron absorber has high thermal conductivities. The TC in the parallel direction of the composite region is higher than that for the thickness direction.

TCs of Gd–alloyed DSS increase with temperature and have values between 10.989 $\frac{\mathrm{W}}{\mathrm{m \cdot K}}$ and 17.680 $\frac{\mathrm{W}}{\mathrm{m \cdot K}}$. Those values are higher than TCs of existing neutron absorbers in the thickness direction. In this study, 0.7 wt.% Gd–alloyed DSS manufactured by casting was considered in the thermal analysis. Yet, the existing neutron absorber for the parallel direction still showed excellent thermal conduction, approximately 3 times that for Gd–alloyed DSS. Therefore, it is necessary to confirm the effect of the neutron absorber in the spent fuel cask.

2.3 Boundary condition

The heat transfer mechanism in the casks consists of conduction, convection and radiation, as shown in Figure 19. Heat transfer mechanism in a spent fuel cask In the spent fuel assembly region, radiation and conduction are known as the dominant heat transfer methods [34]. The decay heat removal system is also affected by the thermal conduction of the cask components. On the cask surface, the natural convection of air and radiation heat transfer dominate (see heat transfer equation below).

$$q'' = h(T_{sur} - T_{amb}) + \sigma\epsilon(T_{sur}^4 - T_{amb}^4)$$

In this section, the boundary conditions are described in order to simulate heat transfer. The boundary conditions include the decay heat from each SNF assembly and the external conditions on the cask surface. Thermal integrity should be evaluated as normal, abnormal, fuel loading or accident conditions. In the case of this study, thermal evaluation was performed only under normal condition.

2.3.1 KSC-1

The fuel region in the KSC-1 cask was assumed to contain 12 fuel rods. The design basis fuel was considered as 16X16 PLUS7, with the calculated maximum decay heat of the fuel rods as 187 W [35]. The volumetric heat generated from the 12 fuel rods was applied as 55700 W/m^2.

The transportation cask containing radioactive materials should consider the effects of solar radiation. The absorbed solar radiation varies depending on the surface shapes (cylindrical or flat surfaces) and surface angles (vertical or horizontal surfaces). According to 10 CFR 71, the absorbed solar radiation on the cask surface is shown in Table 10. The ambient temperature used was 38 ℃ [13]. In order to consider radiative heat transfer on the cask surface, emissivity was also considered. Emissivity of stainless steel has a range between 0.1 and 0.8. In this thermal analysis of KSC-1, an emissivity of 0.5 was applied to the cask surface. The heat transfer coefficient of air-flow on the cask surface was applied using the correlation of the temperature difference between the cask surface and the ambient, as shown below [23, 36].

$$h = 1.24(T_{sur} - T_{amb})^{\frac{1}{3}}$$

2.3.2. KORAD-21

The decay heat applied to each fuel assembly region was used as the maximum value calculated for the fuel assembly which has 45000 MWD/MtU for burnup and 3.0 wt.% for enrichment. The peaking factor along the axial direction of the fuel assembly was applied. It has between 1.1 to 1.2 times the average value at the intermediate region, yet sharply decreased at both ends [37]. Under normal conditions, the ambient temperature of the storage cask is recommended in order to apply the maximum temperature of the mean annual temperature. According to data from the Korea Meteorological Agency, the maximum annual average temperature is 22 ℃, which was applied to the analysis. The storage cask should take into consideration solar radiation, like that of the transportation cask. Since the thermal inertial is large for the storage cask, it is possible to take a 24–hour average value of the solar radiation used in the transportation cask. The values of the solar radiation applied to the cask surface are as shown in Table 11. Buoyancy force plays a major role in maintaining natural convection flow. In order to determine the natural convection characteristic on the cask surface, Ra, which represents the ratio between the fluid buoyant force and the viscous force, was calculated.

The horizontal flat surface;

$$Gr_D = \frac{buoyant\ force}{viscous\ force} = \frac{g\beta\Delta T D^3}{v^2} = 1.41 \times 10^9(\Delta T)$$

$$Ra = Gr_D \times Pr = 1.41 \times 10^9(\Delta T) \times Pr = 1.01 \times 10^9(\Delta T)$$

The vertical curved surface;

$$Gr_L = \frac{buoyant\ force}{viscous\ force} = \frac{g\beta\Delta T L^3}{v^2} = 2.17 \times 10^{10}(\Delta \mathrm{T})$$

$$Ra = Gr_L \times Pr = 2.17 \times 10^{10}(\Delta \mathrm{T}) \times Pr = 1.55 \times 10^{10}(\Delta T)$$

It is common to correlate the occurrence of a natural convection transition using the Rayleigh number, with the transition to turbulence being applied when the Ra value is in the 10^9 scale. For turbulent natural convection, the Nusselt number (Nu), which is the ratio of convection and conduction heat transfer, can be described as below [29].

$$\mathrm{Nu_D} = 0.10 \cdot (Gr_D \cdot Pr)^{\frac{1}{3}} \text{ ; for the horizontal flat surface}$$

$$\mathrm{Nu_L} = 0.15 \cdot (Gr_L \cdot Pr)^{\frac{1}{3}} \text{ ; for the vertical curved surface}$$

Using the relationship between the thermal conductivity and the Nusselt number, the convection coefficient on the cask surfaces were defined as follows.

$$\mathrm{Nu} = \frac{h \cdot l}{k}$$

The horizontal flat surface

$$\mathrm{h_D} = \left(\frac{k_{air}}{D}\right) \times 0.15 \cdot \{1.01 \times 10^9 (\Delta T)\}^{\frac{1}{3}} = 1.82 \times \Delta \mathrm{T}^{\frac{1}{3}}$$

The vertical curved surface

$$\mathrm{h_L} = \left(\frac{k_{air}}{L}\right) \times 0.10 \cdot \{1.55 \times 10^{10} (\Delta T)\}^{\frac{1}{3}} = 1.21 \times \Delta \mathrm{T}^{\frac{1}{3}}$$

2.4 Solver setting

FLUENT solves continuity, momentum, and energy conservation equations for heat transfer calculations. In FLUENT, the flow variables are stored at the center of the mesh cells based on the control volumes. The pressure-based coupled solver (PBCS) was applied to solve the variables. It requires about 2 times more memory than the pressure-based segregated solver because the coupled solver solves pressure and momentum equations simultaneously [38]. However, it takes less time to converge. In order to solve the problems, the second-order upwind was used as an interpolation scheme for the momentum and energy equations. The least squares cell–based approach for gradients was used. To solve for the natural convection in the cavity, the body-force-weighted scheme for calculating cell-face pressures was applied.

2.5 Analysis method verification

The thermal analysis of the KSC-1 model followed normal transportation condition, while the KORAD-21 model was based on the normal storage condition. Calculation results used for thermal evaluation should be validated with the actual data. Instead, verification of analytical method was performed due to the lack of the actual data by comparing the calculated temperatures with those in the reports performed under the same conditions. The relative temperature differences (θ) can be calculated as follows [39].

$$\theta(\%) = \frac{T_{cal} - T_{rep}}{T_{rep} - T_{amb}} \times 100$$

2.5.1 KSC-1

Based on the previously mentioned scenario and boundary condition, the thermal analysis of the KSC-1, which uses stainless steel as a basket, was conducted. By monitoring the maximum temperature of fuel cladding, shown in Figure 21, it was confirmed that the cladding temperature converged at 70.6 ℃. Figure 22 shows the temperature distribution of the KSC-1 cask. In order to compute the temperature differences, the components were selected as shown in Table 12. The maximum temperatures were extracted from each component region. The calculated maximum temperatures of the components were compared with the results described in the SAR KSC-1. The most apparent difference amongst the calculated values was -3.4 % for the cask surface temperature. However, it is still similar with the values in the report. The result of the calculated temperature differences means that the calculation results are within reasonable ranges, and the thermal analysis method well verified.

2.5.2 KORAD-21

The thermal analysis of the KORAD-21 cask was also performed based on the scenario described for the spent fuel storage cask. In the evaluation, the existing neutron absorber with BORAL was considered as the basket in the KORAD-21 cask. Figure 23 shows that the cladding temperature was confirmed as 369.7 ℃ at convergence. The calculated temperature of fuel cladding has a difference of 8.7 ℃ between the resulting and the reported value, yet the temperature difference is 2.5 %, which is within a reasonable range. The largest temperature difference is represented by -3.6 % in the cask body, yet it can be concluded that the thermal analysis is proven because all values are within a 5 % margin of error.

III. Results & Discussion

3.1 Adoption of Gd-alloyed DSS as neutron absorber and structure material

3.1.1 KSC-1

KSC-1 uses stainless steel as a basket without a neutron absorbing material. In this section, Gd-alloyed DSS was adopted as basket material instead of stainless steel so as to evaluate thermal effect of the Gd-alloyed DSS on spent fuel cask. Thermal analysis was conducted on the aforementioned normal condition for transportation cask. The calculated temperature distribution is shown in Figure 27. The average temperature of the water was approximately 67.0 ℃. The maximum temperature of the fuel cladding surface at the center of the fuel rod was calculated to be 70.6 ℃. It displays the natural convection by water in the cavity and indicates that the temperature difference between the fuel surface and the water is not large. The maximum temperature of the lead shield was calculated as 66.4 ℃, which did not exceed the melting point for lead of 327.0 ℃. The calculation results are much lower than the allowable temperatures. The ethylene-glycol solution was mixed fifty-fifty with water in order to act as a neutron shield. Since the freezing temperature of the ethylene-glycol mixture is -40.6 ℃, 40.0 ℃ was selected as criteria for the ethylene-glycol mix. Therefore, the KSC-1 cask with Gd–alloyed DSS satisfies safe operating temperatures under normal conditions. In addition, the results of the cask with the Gd–alloyed DSS are similar with the previously calculated results of KSC-1 because thermal properties of Gd-alloyed DSS are similar with the stainless steel. The calculated Ra number, based on the temperature result, has a value ranging from 3.8×10^8 to 7.5×10^8.

3.1.2 KORAD-21

The thickness of the conventional neutron absorber having composite structure, including the inner stainless steel of 5.0mm, BORAL and the outer stainless steel, is 9.5mm. The Gd-alloyed DSS was adopted in KORAD-21 cask and thermal analysis was performed with a 9.5mm basket wall thickness. Thermal performance of the Gd-alloyed DSS case and the BORAL case was compared. The temperature distribution of the Gd-alloyed DSS and the BORAL case in the same thickness is shown in Figure 30 and Figure 31 respectively, using the same temperature scale. It is clearly visible in the temperature distribution that internally generated decay heat is high in the 9.5 mm Gd–alloyed DSS case. The maximum temperatures of the 9.5mm Gd-alloyed DSS case were calculated as shown in Table 15. The results of the 9.5 mm Gd–alloyed DSS case are higher than that for the BORAL case, except for the cask lid. In particular, the fuel cladding temperature of the 9.5mm Gd-alloyed DSS case was 414.4 ℃, which exceeded the allowable temperature of 400.0 ℃. This can affect the fuel integrity and result in

rupture of fuel cladding by thermal creep. There are limitations on adoption of Gd-alloyed DSS in the KORAD-21 cask. Not only the fuel cladding temperature but also the basket, and disk temperatures have been influenced is about 45.0 ℃ higher than that for the BORAL case. It seems that the thermal conductivity of different neutron absorbing material affected the thermal performance. The radial thermal conductivity of the Gd-alloyed DSS are bigger than that of BORAL case. The axial thermal conductivity of the BORAL case is about four times that of the Gd–alloyed absorber. Although it may remove the decay heat in the basket for the thickness direction, it seems that the heat transfer in the axial direction affects the performance.

3.2 Design optimization of UNIST design cask

3.2.1 Basket wall thickness optimization

According to the previous results, the KORAD-21 cask with the Gd-alloyed DSS of 9.5mm wall thickness did not satisfy safe operating temperature. Therefore, this work is intended to optimize the cask design with Gd-alloyed DSS based on thermal performance. The KORAD-21 cask has disk structures inserted along the basket in the axial direction at intervals. There is a gap between the basket structure and the disk square holes, as shown in Figure 32. The basket wall thickness of Gd-alloyed absorber case can be reduced with reflection the gain from increased neutron absorption by Gd. When the basket wall thickness was reduced to 5.0mm from 9.5mm, the gap increases to 7.5mm (5.0mm basket wall thickness) from 3.0mm (9.5mm basket wall thickness). Even the same material can affect decay heat removal capability depending on the basket wall thickness. Figure 34 shows that natural convection of helium and its velocity distribution for the 5.0mm and 9.5mm basket wall thickness cases. When the gap is magnified in the flow distribution, it confirms that the flow velocity of the 5.0mm case is higher than that of the 9.5mm case. Velocity streamline, as shown in Figure 35, reveals that the flow into the gap has upward flow pattern. In short, the increase of gap helps the upward flow become more active. In order to compare the flow effect for two cases numerically, the averaged Nusselt number, which indicates the ratio of convective to conductive heat transfer, was calculated on the basket outer surface. The averaged Nusselt number of the 5.0mm and 9.5mm case were calculated as 4.5534 and 3.5576, respectively. Since the thermal conductivity of the helium on the basket surface hardly changes, it means that the high Nu number is affected by the convective heat transfer coefficient.

Thermal performance of the 5.0mm basket wall thickness with Gd-alloyed DSS was evaluated. The calculated results are shown in Table 16. In particular, the maximum temperature of fuel cladding is calculated as 389.9 ℃. The results of other components are also within the allowable temperatures and smaller than the results of the 9.5mm case. The temperature distributions of the 9.5mm and 5.0mm wall

thickness case with the same temperature scale are shown in Figure 30 and Figure 33 respectively. Figure 30 displays that temperature is higher in the center of the cask than the results of the 9.5mm case which was previously calculated. In addition, temperature distribution showed that the position, that maximum decay heat appeared, was differently shown as 3.342m (the 5.0mm case) and 3.001m (the 9.5mm case). It means that the upward flow, which resulted from the gap increase, enhanced decay heat removal capability. Therefore, when using Gd–alloyed DSS, the 5 mm wall thickness is more effective in removing decay heat than the 9.5mm case.

3.2.2 Disk thickness optimization

With regard to thermal effect of basket wall thickness, it was derived that the 5.0 mm wall thickness of Gd–alloyed DSS is effective for removing decay heat. Nevertheless, the performance of that is lower than the BORAL case. In this part, thermal effect of as increase of its thickness was evaluated so as to enhance thermal performance with increase of the heat-conducting surface, and to optimize disk thickness. The KORAD-21 cask, reference cask, has disks of 20mm thickness, but 20, 34, 40, 50 and 60mm was considered for parameter study. In ANSYS FLUENT solver, walls on the disk surface can be created with the shell conduction function, as shown in Figure 36. Calculation results as disk thickness are found in Table 17. Figure 37 shows that the maximum temperature of fuel cladding, basket and disk clearly decrease as increase of disk thickness. The maximum fuel cladding temperature resulted in 357.5 ℃ (60mm) from 389.9℃ (20 mm). However, the results for the cask body and side shield little increased, while those for the cask lid decreased as shown in Figure 38 and Figure 39. This signifies that the increase in heat–conducting surfaces as disk thickness improves radially the heat transfer. As a result, to enhance thermal performance, the optimum disk thickness is 60mm for the cask with the 5.0mm thickness of Gd-alloyed DSS.

However, the increase of disk thickness results in the increase of weight, which can affect the structure integrity for normal and accident scenario such as drop and impact test. If the thickness of the disk increases as 60 mm, 10.6 tons is added and the total weight of the KORAD-21 cask is expected to be 115.1 tons. According to reference, the highest stress in the calculated values was 131.1 MPa for the handling load under normal conditions. However, it was confirmed that the structural integrity within the margin was satisfied with an allowable stress of 241.5 MPa. It seems that an increase of disk thickness does not have a large structural influence in normal condition. The scenario that seems to have the most structural influence under the accident condition is a drop test. The component that has the largest influence on the basket is disk structures. In order to evaluate the specific effect of the cask with the increased weight, additional structure evaluation is required.

3.3 Thermal performance of UNIST design cask with Gd-alloyed DSS

In this study, UNIST design cask was designed based on thermal performance by optimizing basket wall thickness and disk thickness. It was derived that the 5.0 mm wall thickness of Gd–alloyed DSS with 60mm of disk thickness is effective for removing decay heat. Figure 40 presents the temperature distribution of UNIST design cask. The calculation results are shown in Table 18. It can be established that the overall temperature decreased more in the UNIST deign cask case than it did with the BORAL absorber case. The criterion of fuel cladding is 400 ℃, which has been presented in order to prevent gross rupture due to thermal creep. The maximum temperature of fuel cladding was calculated to be roughly 357.5 ℃. This value is about 10 ℃ smaller than the BORAL case of 369.9 ℃. This value is still within the 400 ℃ range. The outer components, based on stainless steel, such as basket, disk, and canister, have a thermal margin compared to the allowable temperature of 427 ℃. The resin used as a neutron shielding material was calculated as 129.0 ℃, indicating that it does not affect the neutron shielding ability. Therefore, the results showed that the safety of the cask using Gd–alloyed DSS is maintained under the normal condition.

IV. Conclusion

Thermal evaluation were conducted for the KSC-1 and KORAD-21 casks, which were selected as reference casks, using ANSYS FLUENT v17. Temperature differences were calculated, and methods used for thermal evaluation were verified.

Thermal properties of Gd-alloyed DSS were measured. The radial thermal conductivity of the Gd-alloyed DSS are bigger than that of BORAL absorber, but the axial thermal conductivity of the former is smaller than the later. Gd-alloyed DSS was adopted in the KSC-1 and KORAD-21. The maximum temperature of fuel cladding in the KSC-1 was calculated as 70.6℃, which results from similar thermal properties with stainless steel. The Gd-alloyed DSS is fully applicable in the KSC-1. In the case of KORAD-21, the 9.5mm wall thickness with Gd-alloyed DSS showed 414.4℃ compared to the BORAL case of 369.7℃. This means that the axial thermal conductivity of the basket affect the decay heat removal capability in the spent fuel cask.

Optimization of the KORAD-21 with Gd-alloyed DSS was conducted. When the basket wall thicknesses of the Gd absorber case was reduced to 5.0 mm which consequently increase the gap to 7.5 mm from 3.0 mm, to reflect the gain from increased neutron absorption by Gd, the upward flow worked effectively as removing the decay heat on the basket surface. The 5.0mm wall thickness case enhanced thermal performance by reducing the maximum temperature of fuel cladding by 389.9℃ (the 5.0mm basket wall thickness) from 414.4℃ (the 9.5mm basket wall thickness).

The effect of disk thickness for the 5mm basket wall thickness case with Gd-alloy was studied. The maximum temperatures of the fuel cladding, basket, and disk clearly decreased as the disk thickness increased. The result of the fuel cladding temperature was reduced by 32.4℃ to 357.5 ℃(60mm thickness) from 389.9℃ (20mm thickness).

In this study, UNIST design cask, which has the 5.0mm wall thickness with Gd-alloyed DSS and the 60mm disk thickness, was developed based on the thermal performance analysis. The maximum fuel cladding temperature of 357.5℃, which is about 12.4 ℃ smaller than the BORAL case of 369.9℃, did not exceed the allowable temperature limit of 400 ℃. Other components also satisfied the allowable values. The UNIST design cask satisfies thermal requirements in normal operation and can provide sufficient decay heat removal capability.

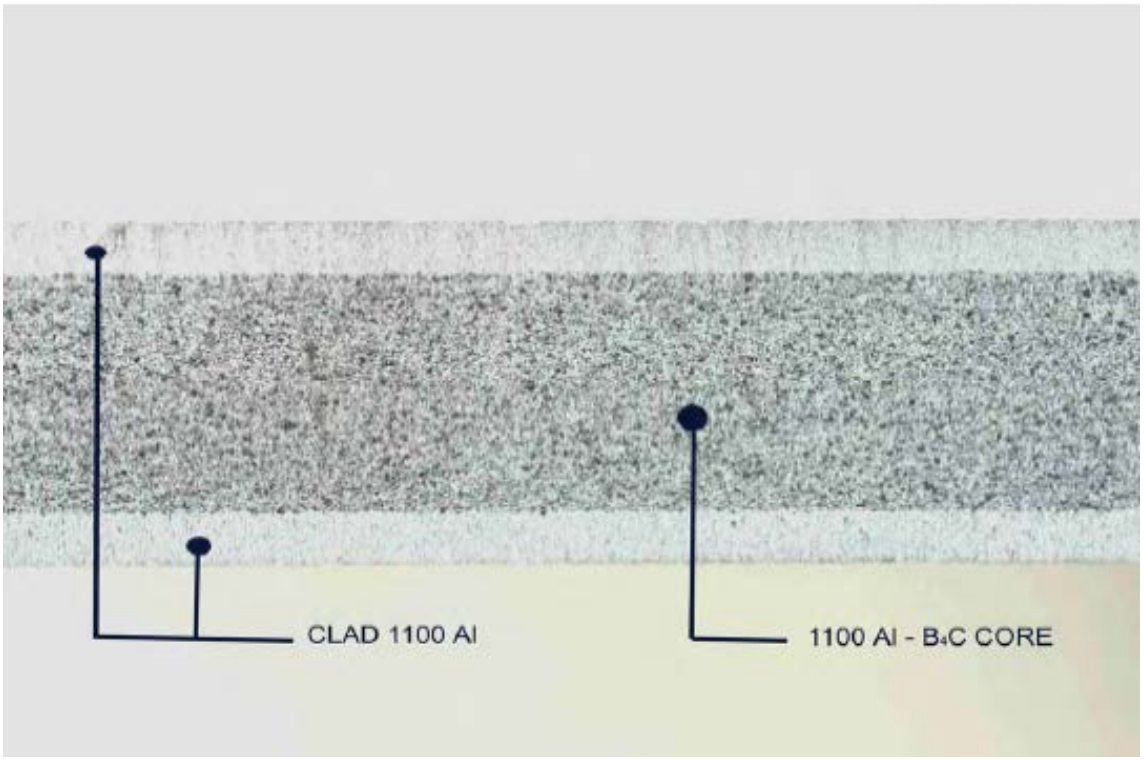

Figure 1. Trimmed edge of BORAL [6]

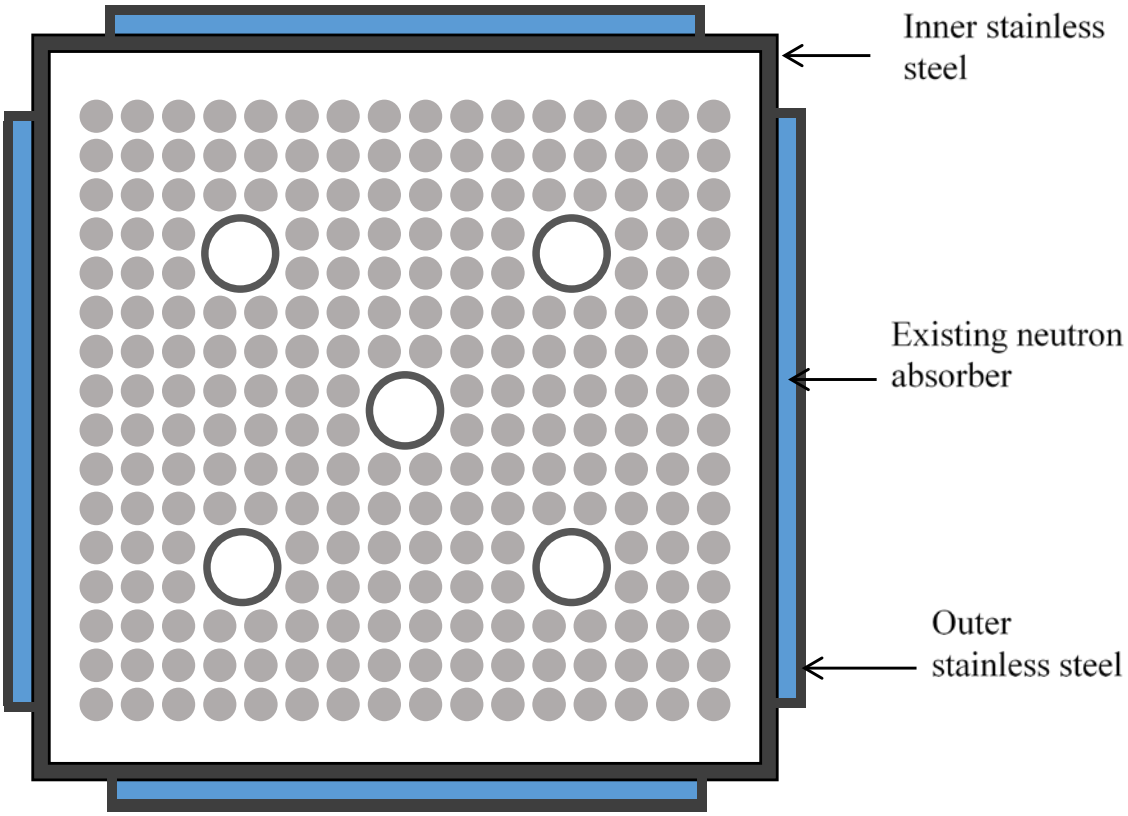

Figure 2. Cross section of a typical basket structure

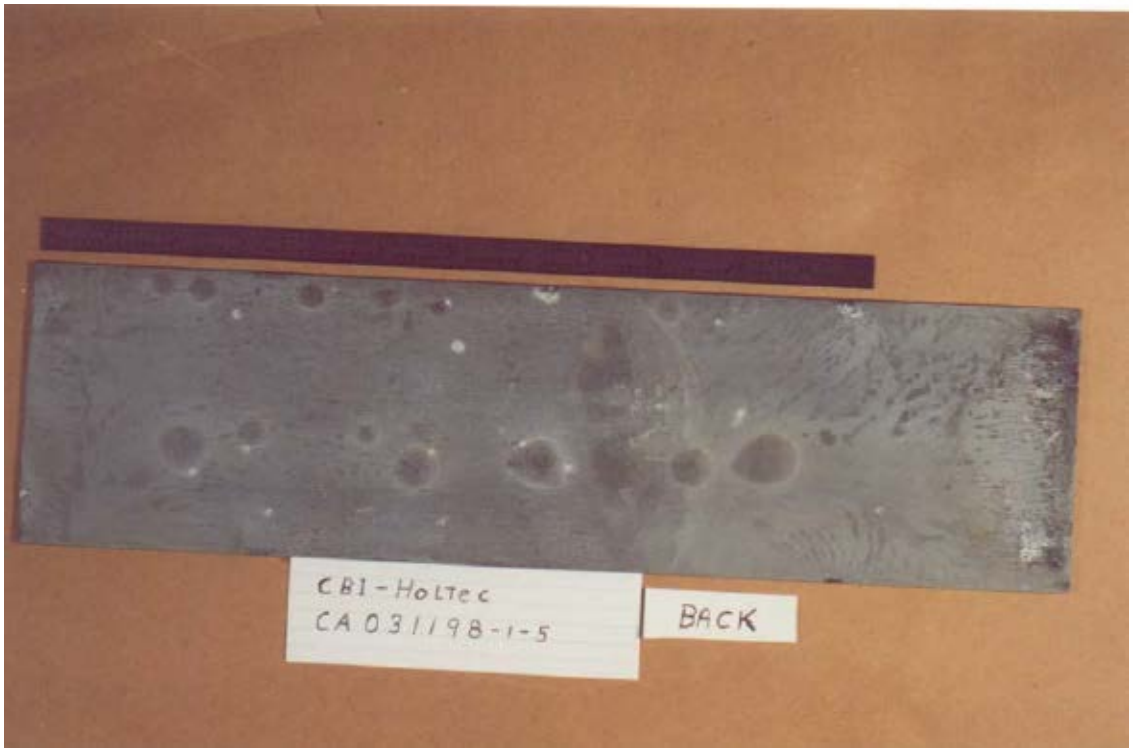

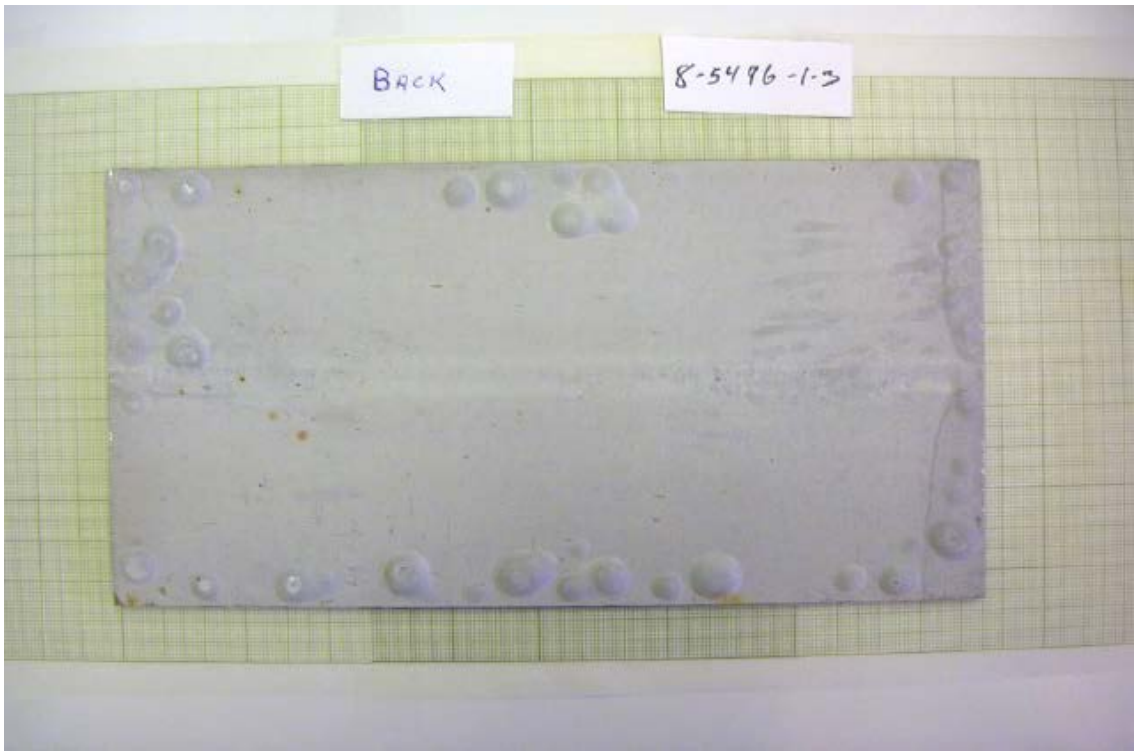

Figure 3. Blister formation on the BORAL surface [4]

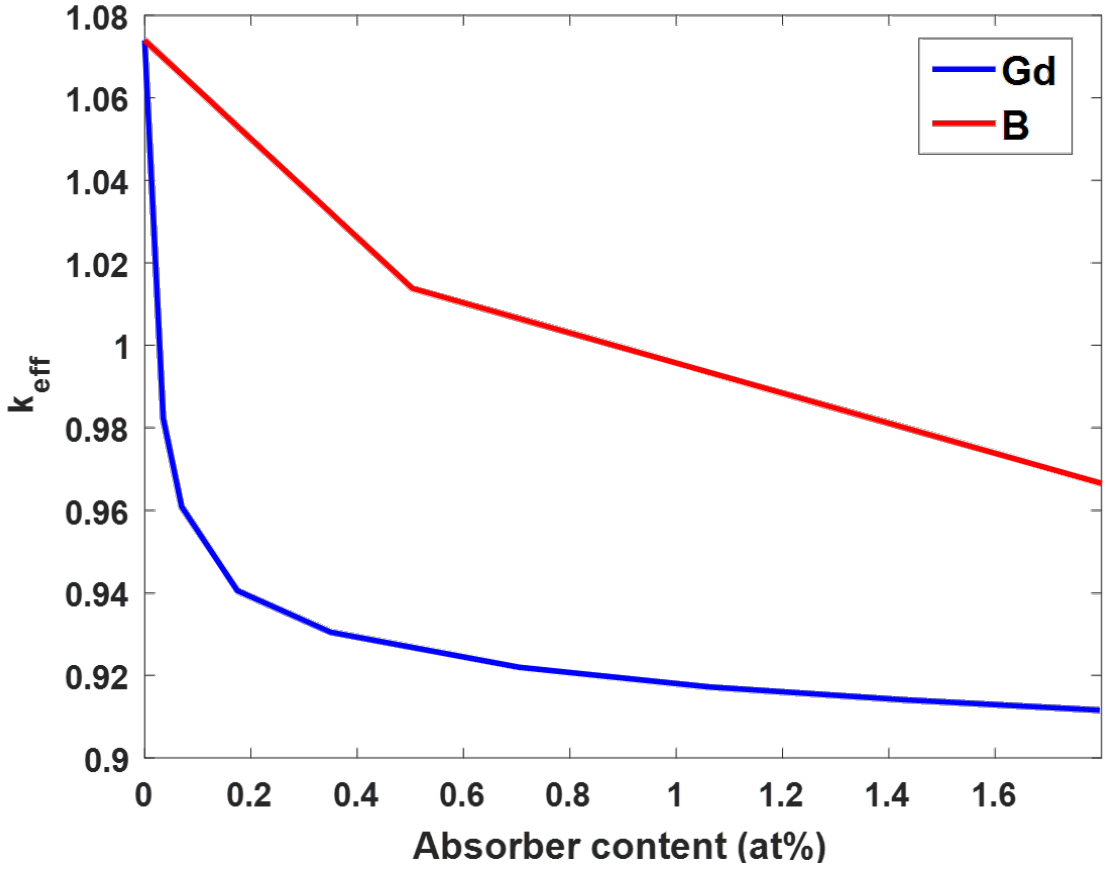

Figure 4. Change of criticality as neutron absorbing material contents [9]

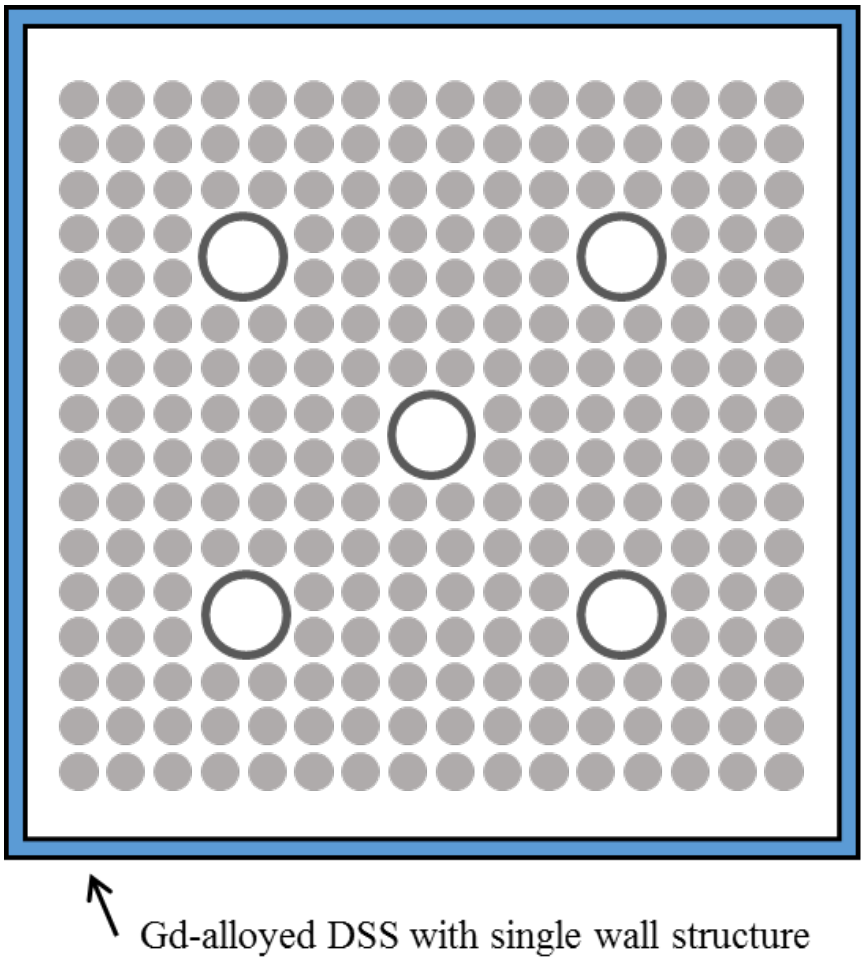

Figure 5. Gd-alloyed neutron absorber having single wall structure

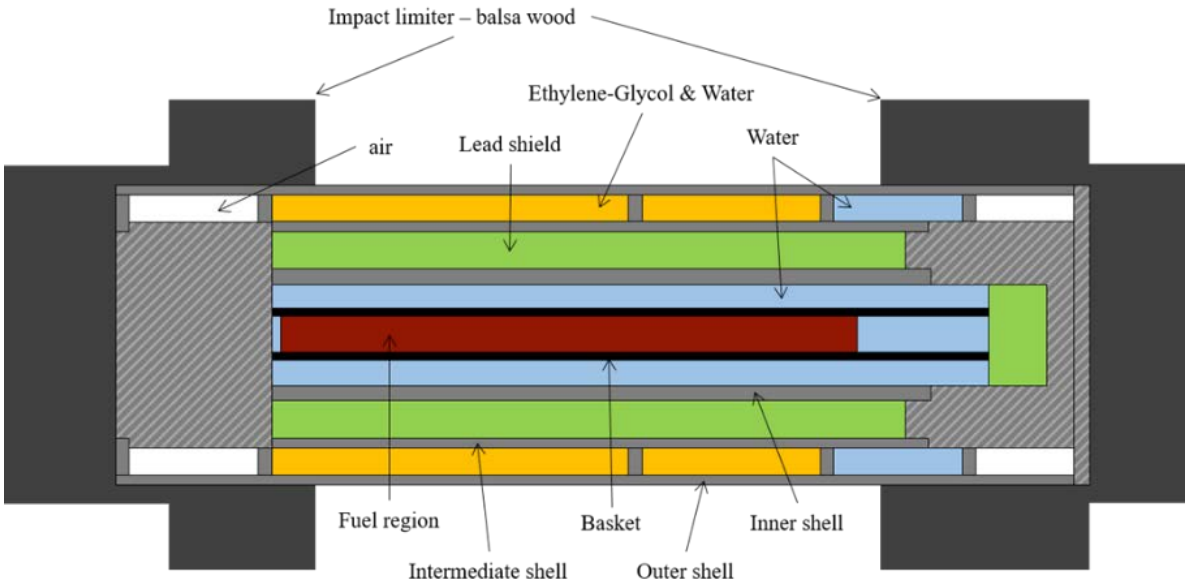

Figure 6. KSC-1 schematic drawing

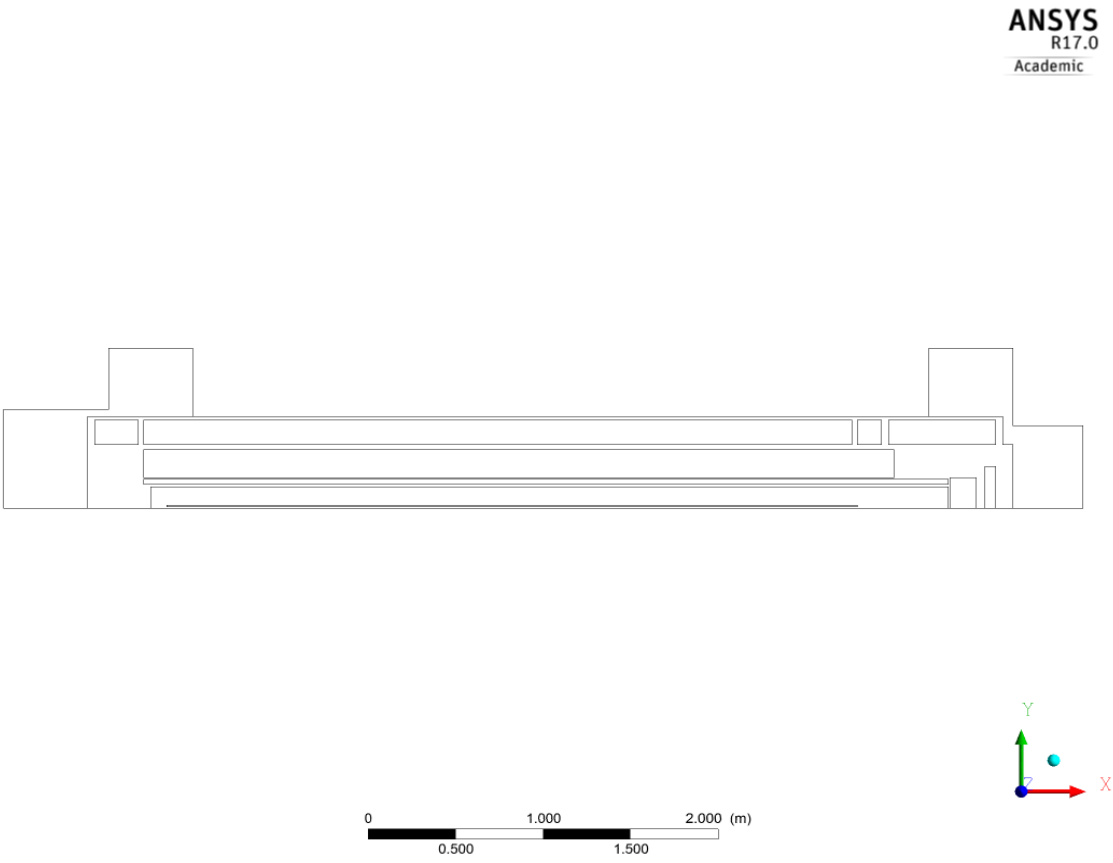

Figure 7. KSC-1 2D axisymmetric modeling

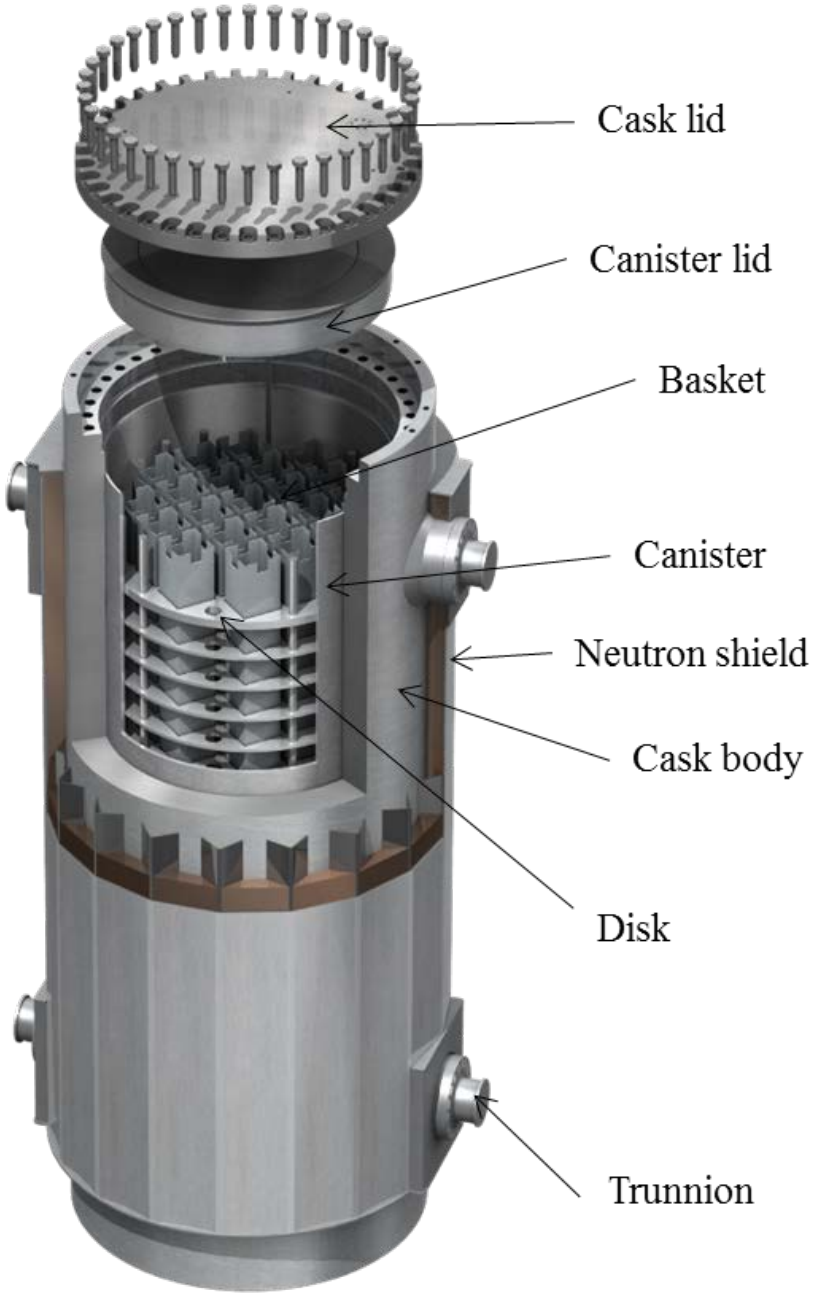

Figure 8. Overall structure of KORAD-21 cask

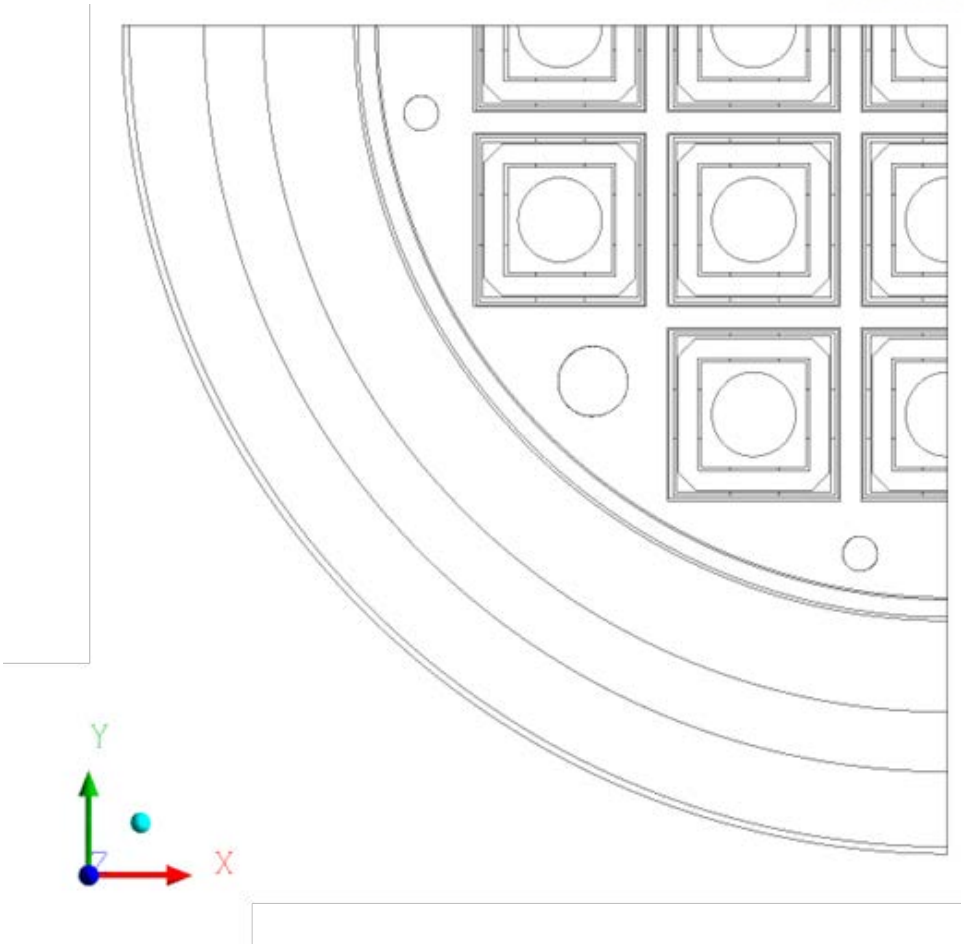

Figure 9. Top view of KORAD-21 modeling

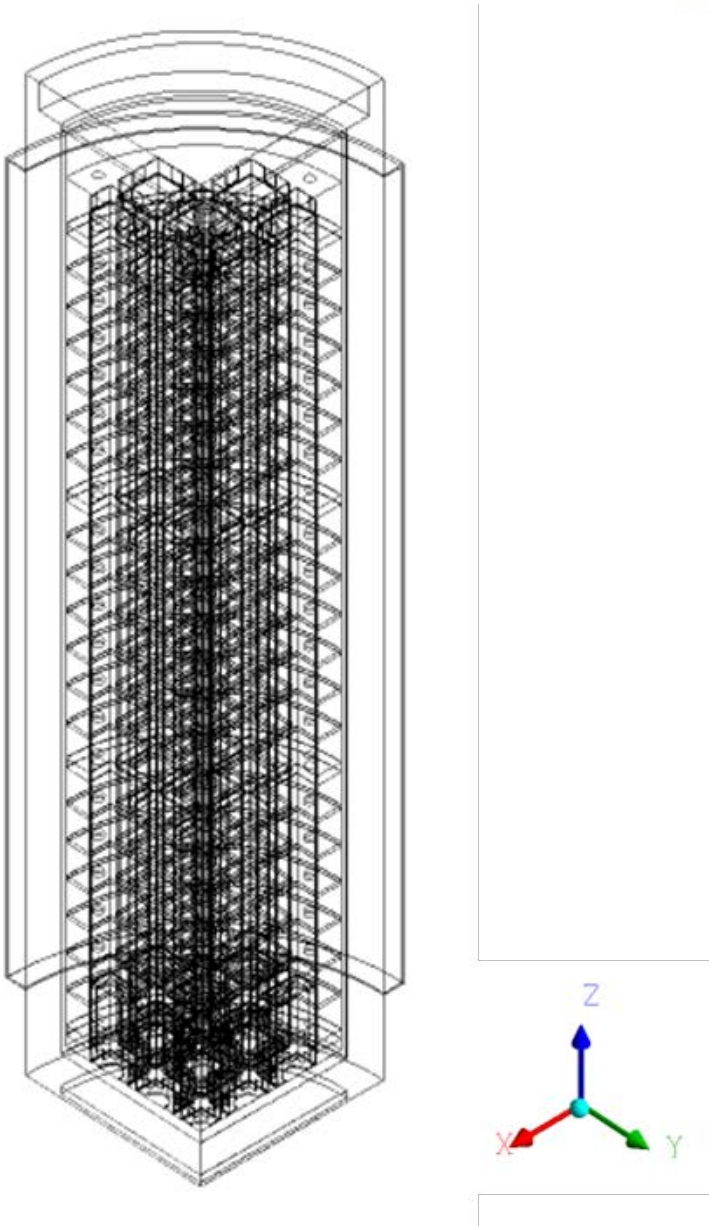

Figure 10. Iso-view of KORAD-21 modeling

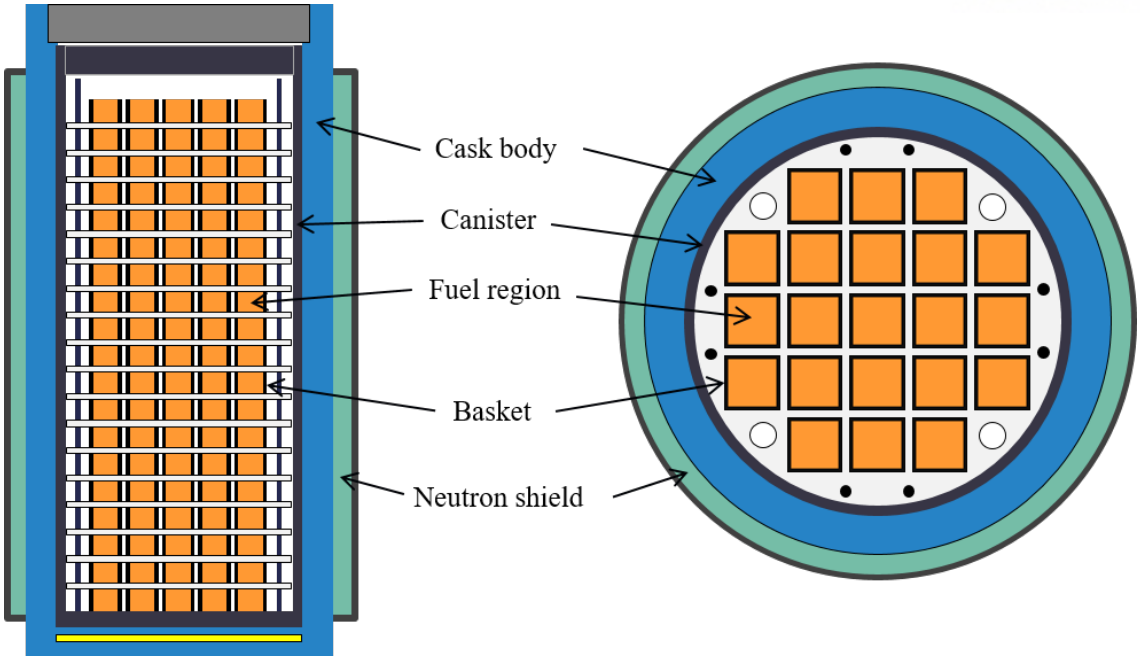

Figure 11. KORAD-21 cask schematic drawing

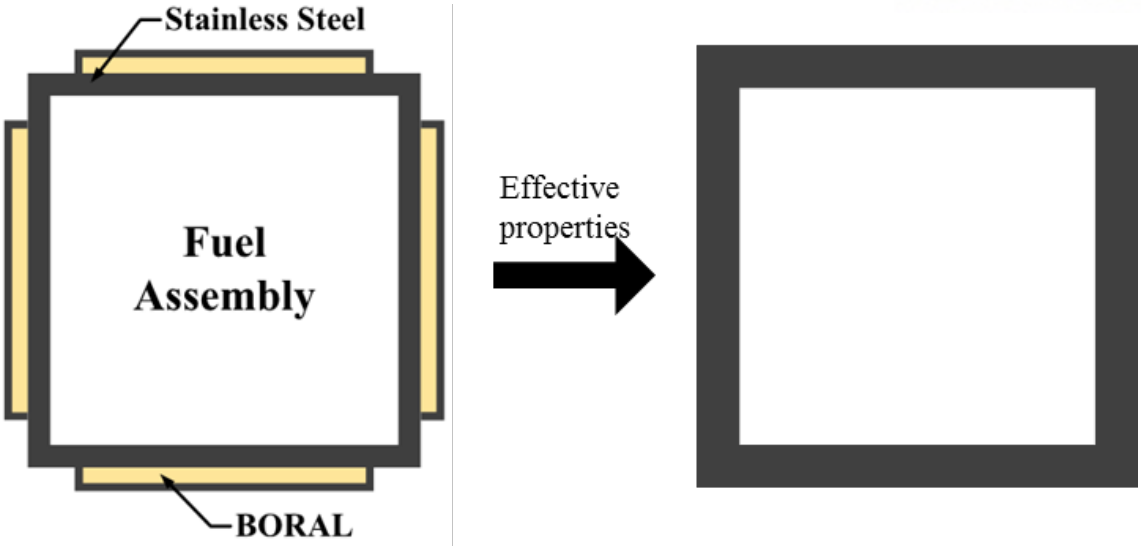

Figure 12. The homogeneous model of composite structure with BORAL

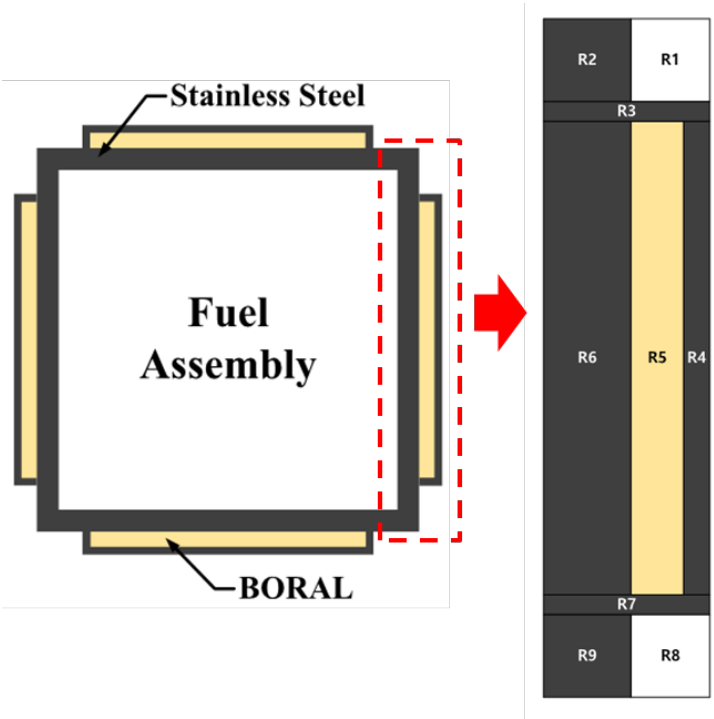

Figure 13. Thermal resistance model of composite structure with BORAL

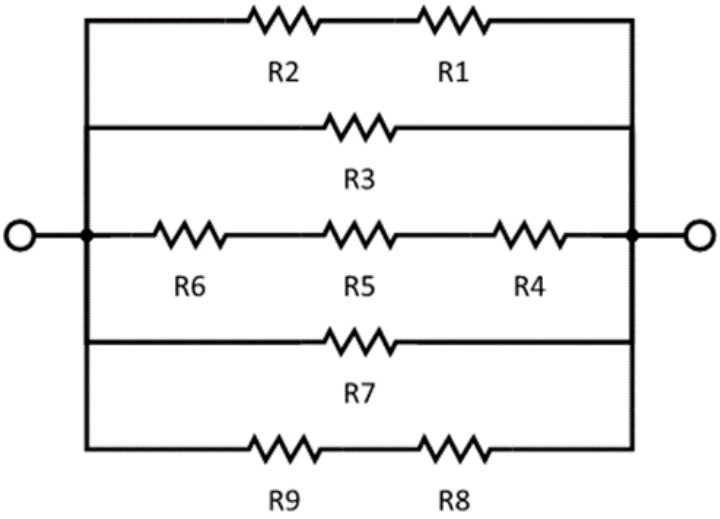

Figure 14. Thermal resistance model for thickness direction

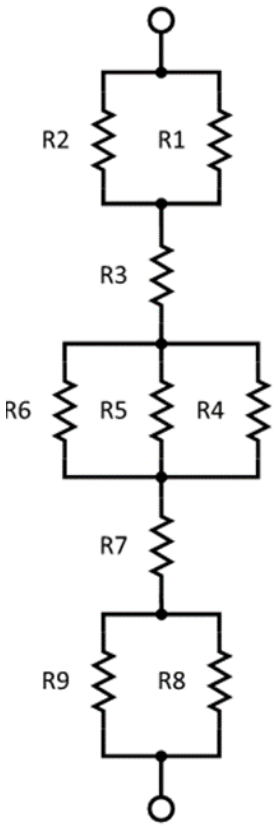

Figure 15. Thermal resistance model for parallel direction

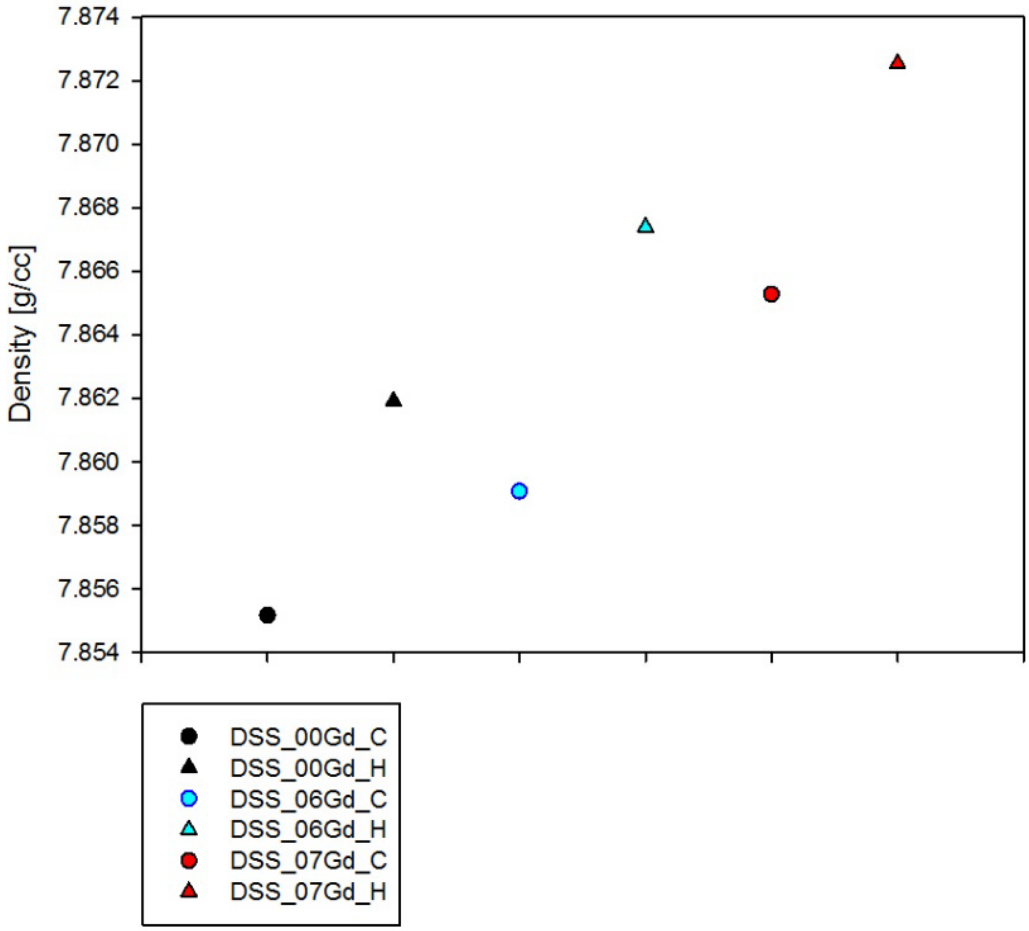

Figure 16. Density measurement results

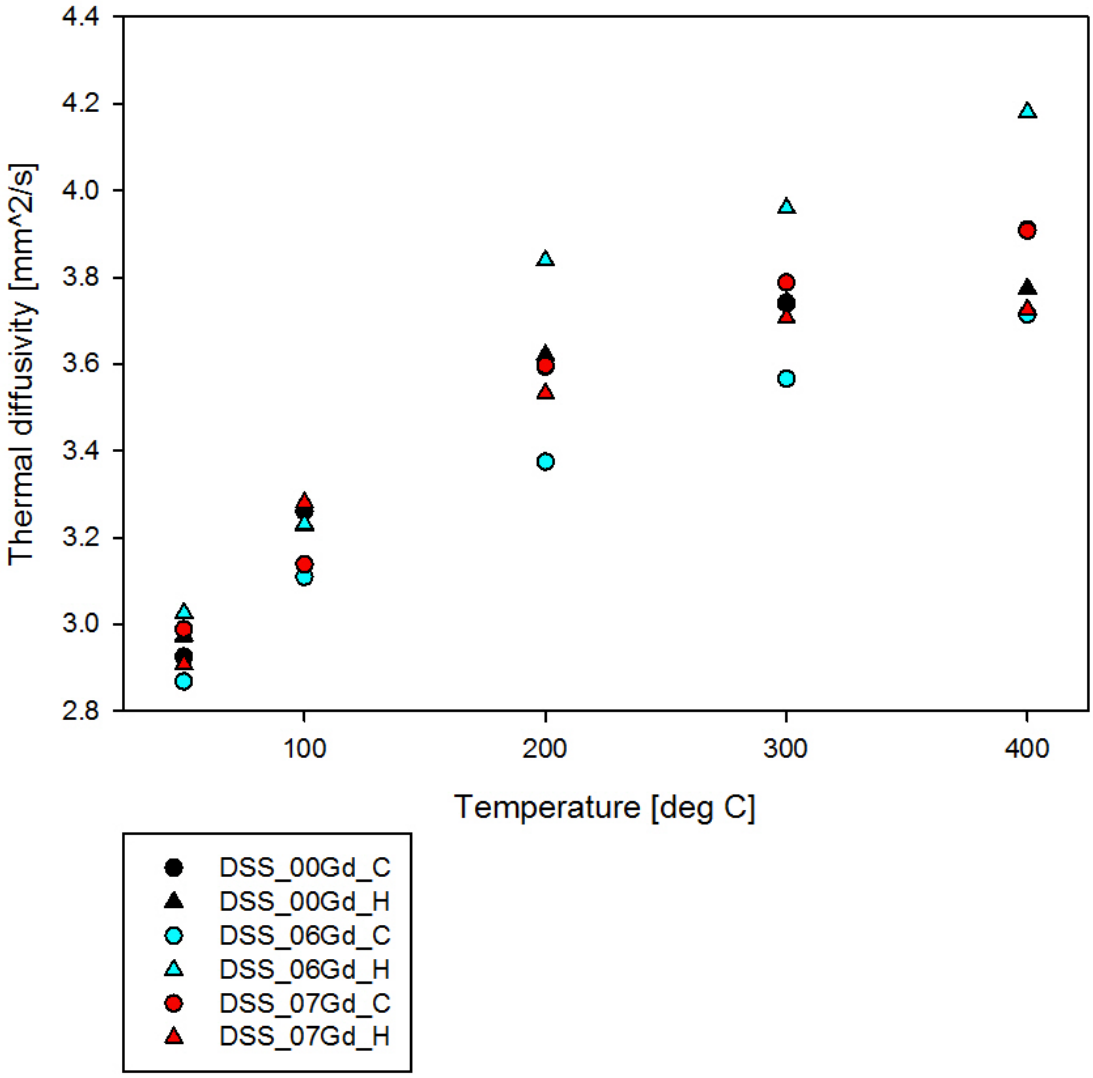

Figure 17. Thermal diffusivity measurement results

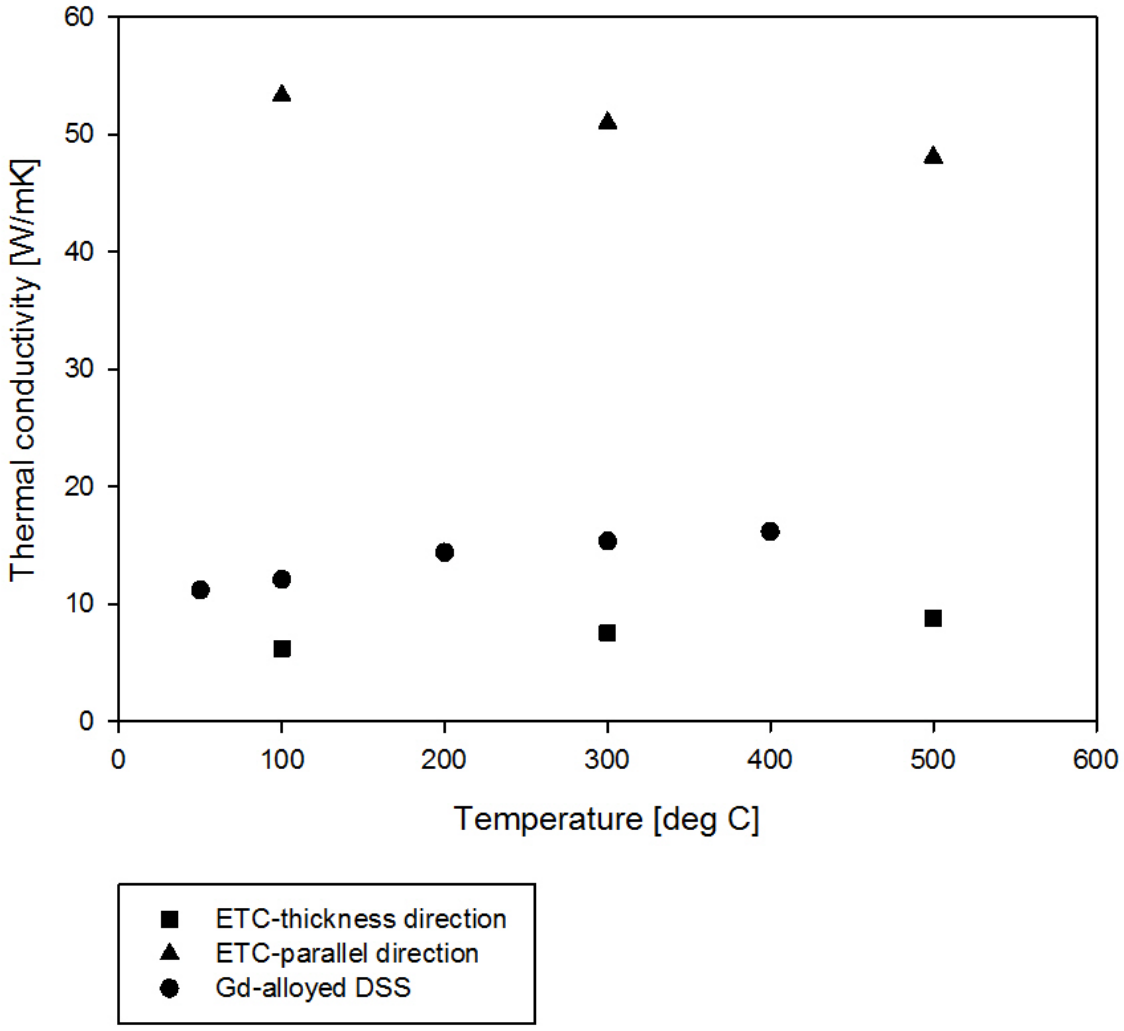

Figure 18. Thermal conductivities of neutron absorbers

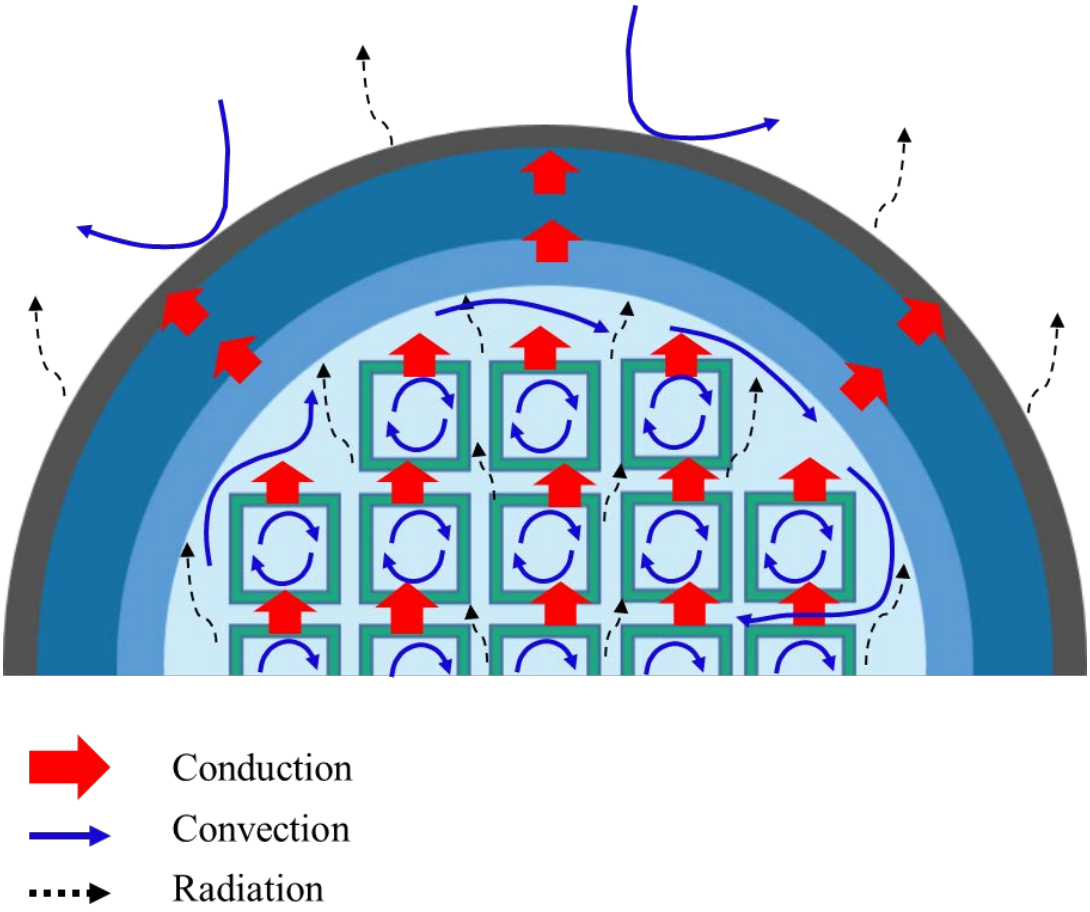

Figure 19. Heat transfer mechanism in a spent fuel cask

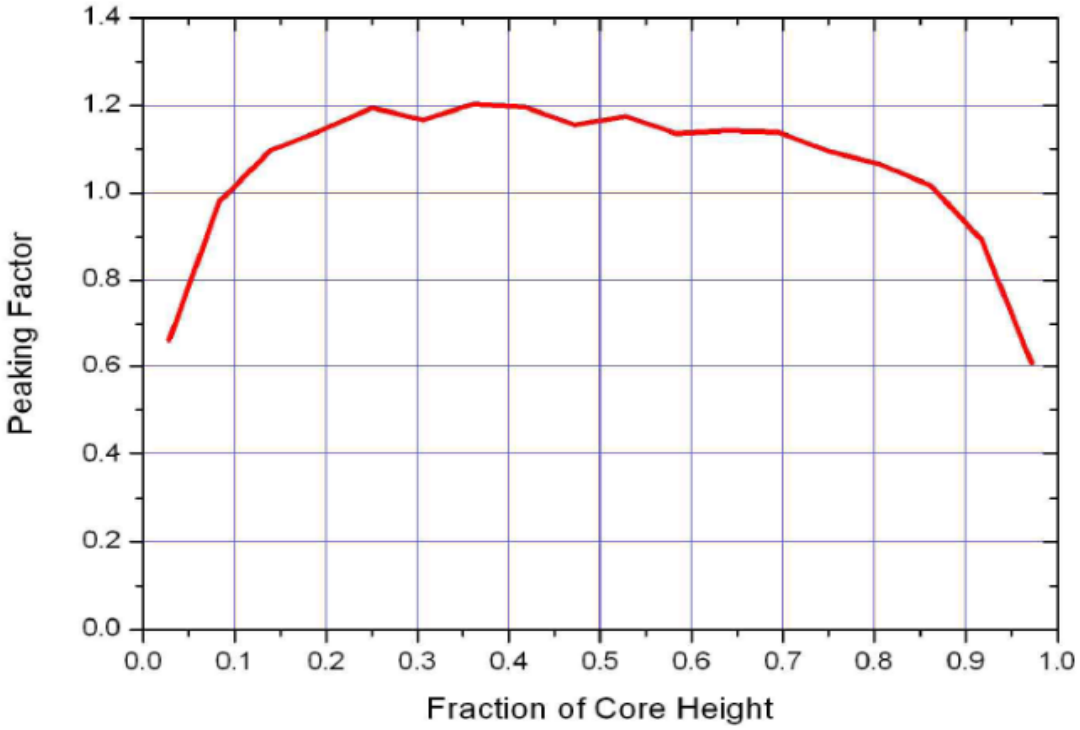

Figure 20. Peaking factor for axial height of SNF [37]

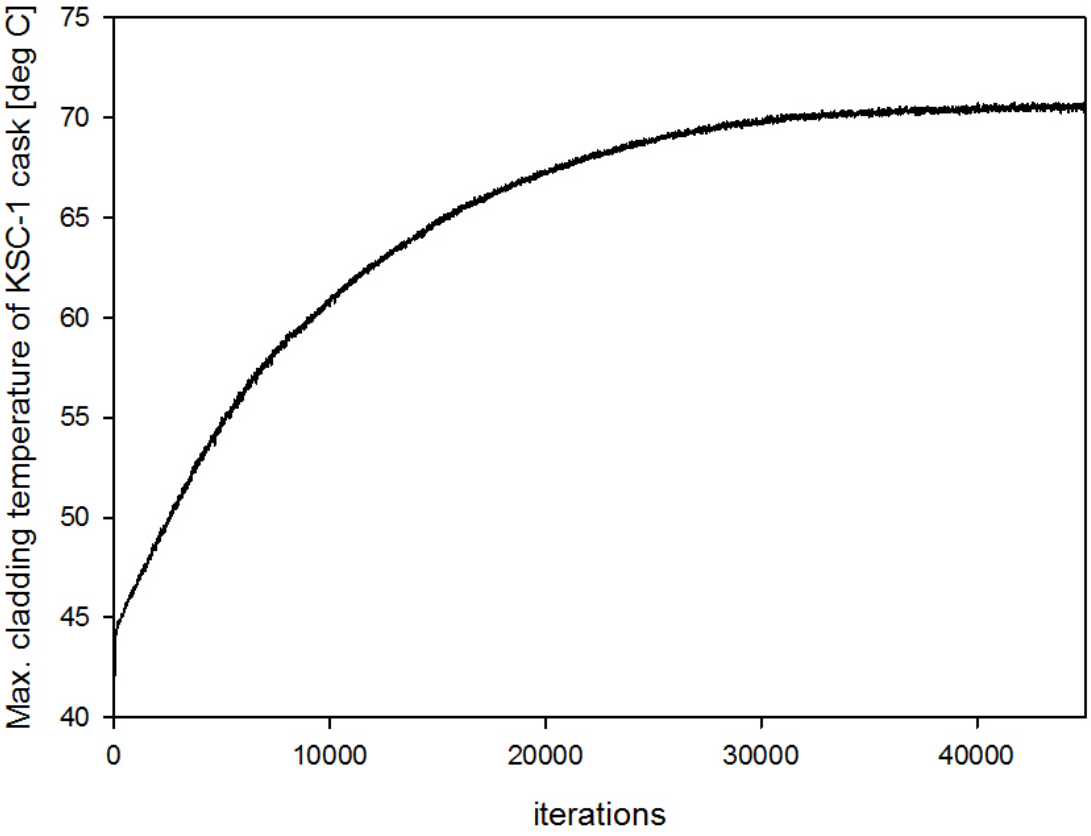

Figure 21. Convergence monitor of cladding temperature in KSC-1;reference case

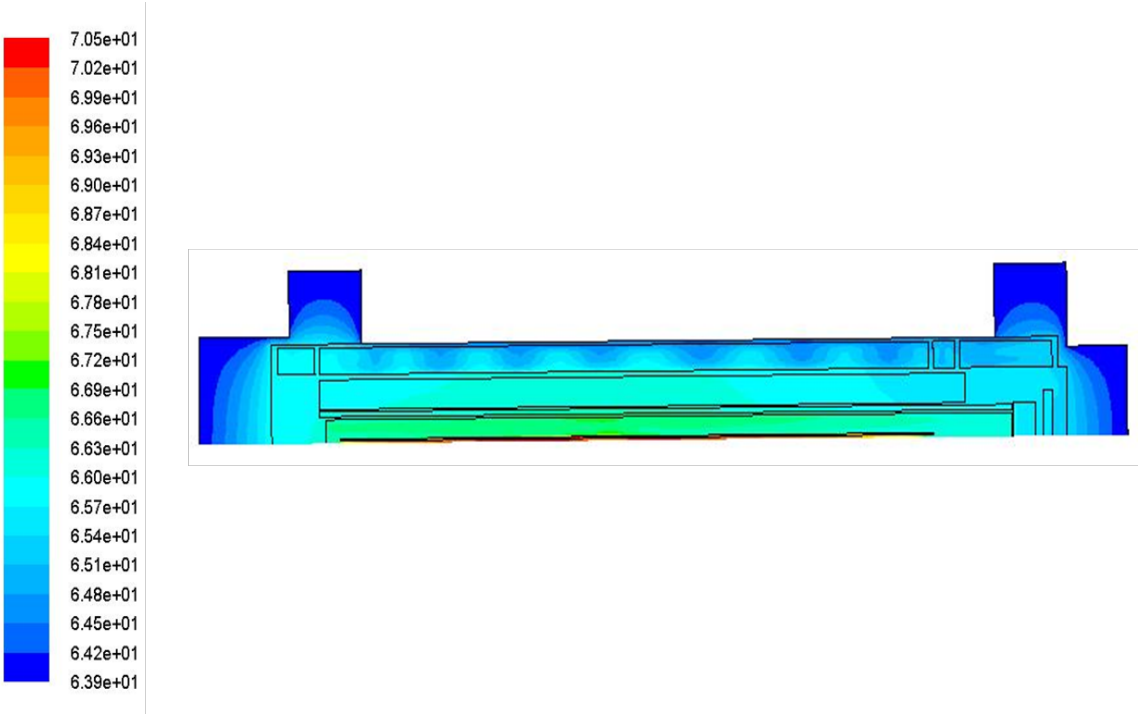

Figure 22. Temperature distribution of KSC-1; reference case

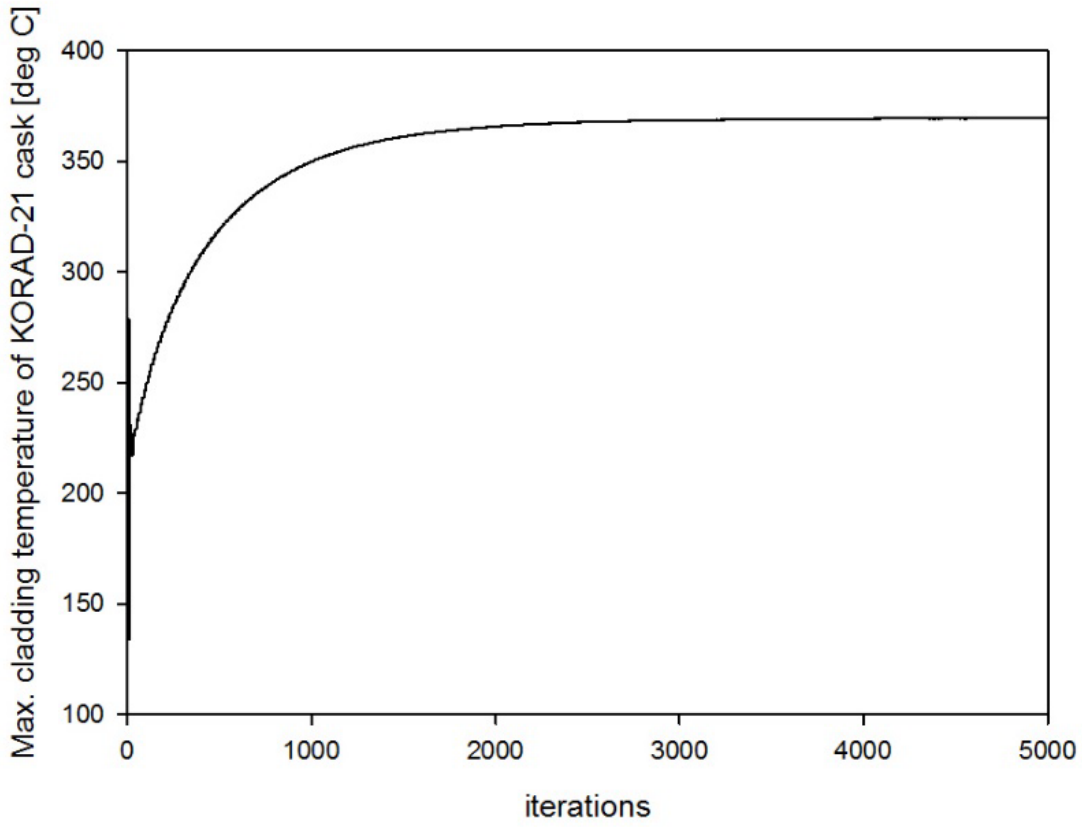

Figure 23.Convergence monitor of cladding temperature in KORAD-21 with BORAL; reference case

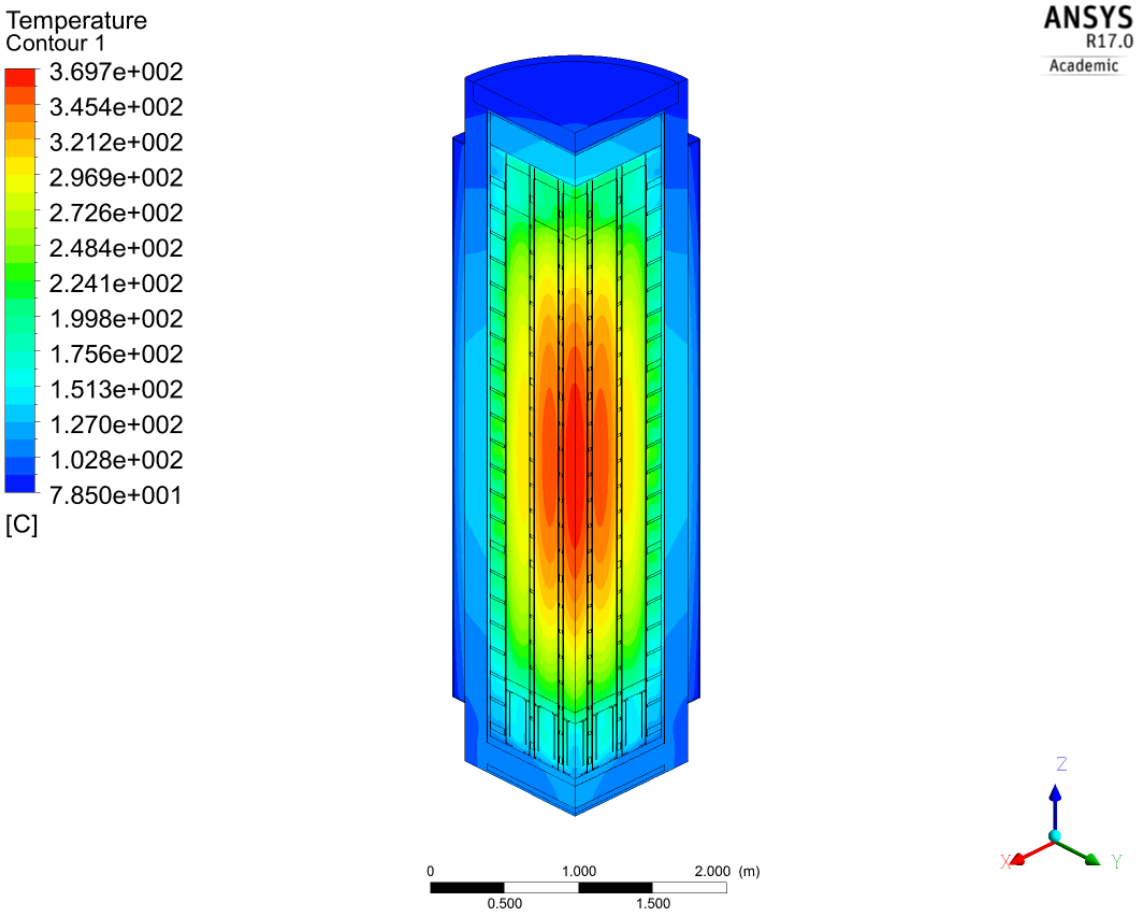

Figure 24. Temperature distribution of KORAD-21 with BORAL; reference case

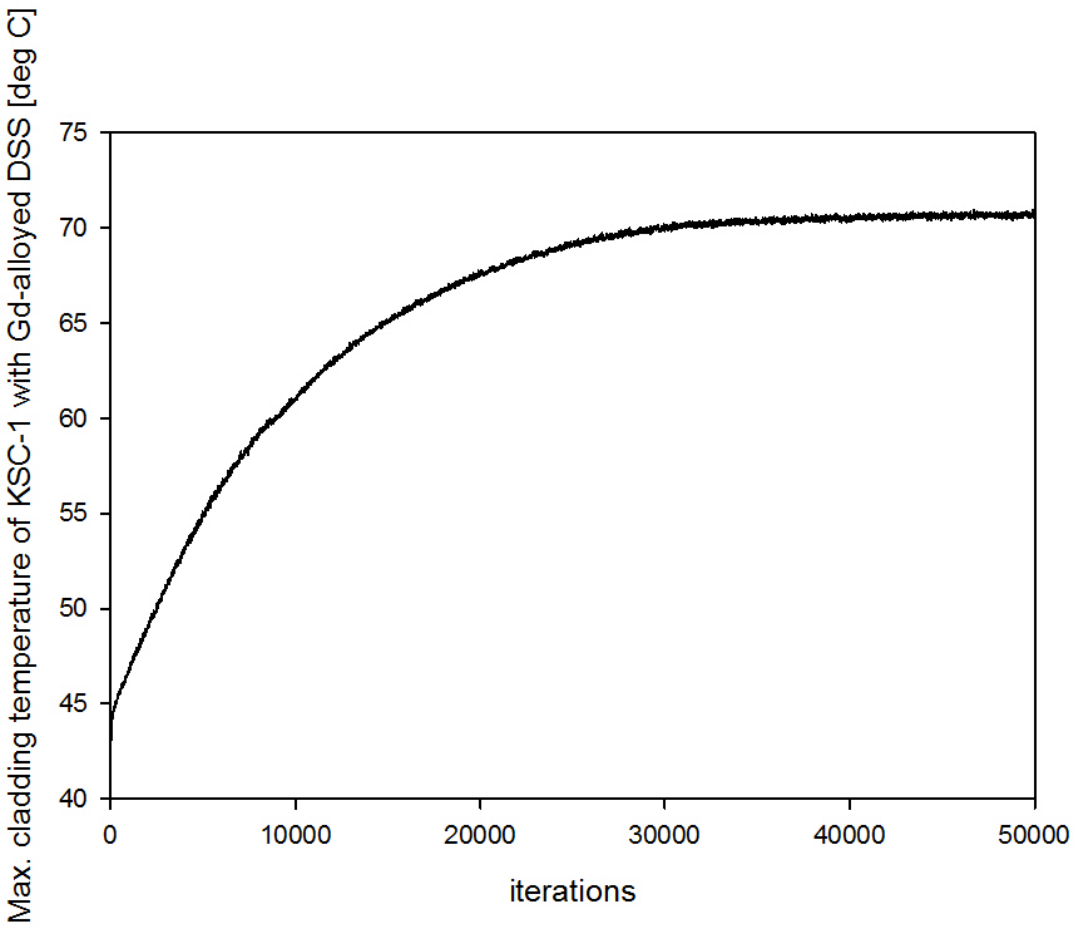

Figure 25. Convergence monitor of cladding temperature in the KSC-1 with Gd-alloyed DSS

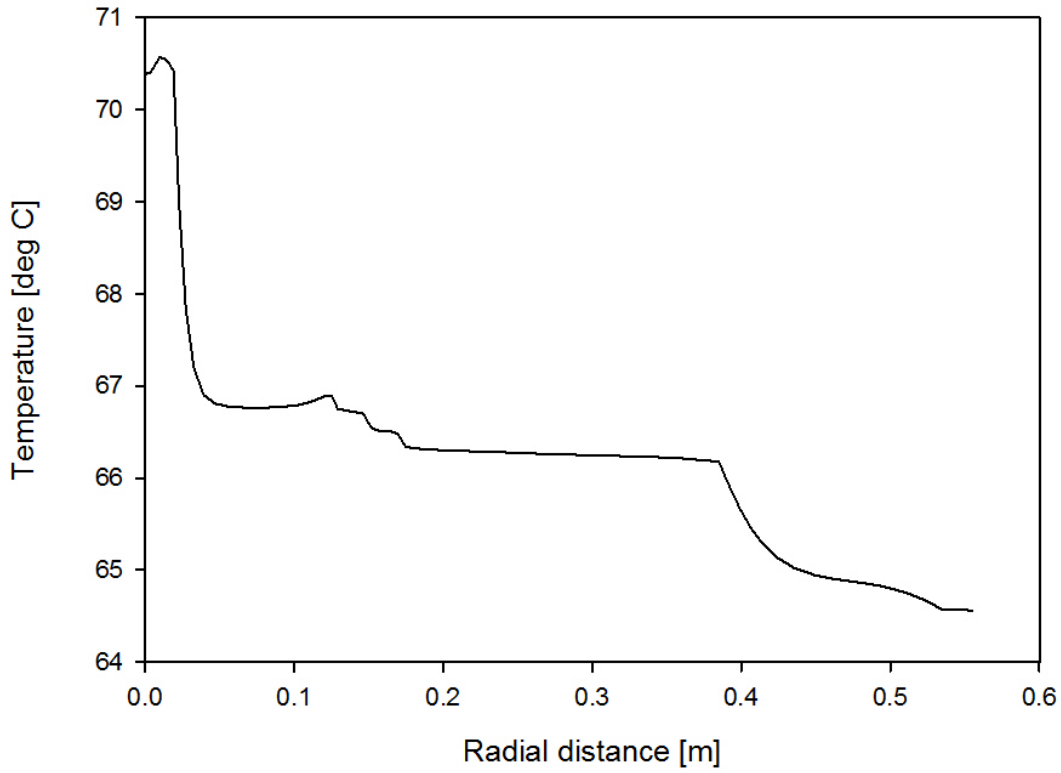

Figure 26. Radial temperature distribution of the KSC-1 which adopts Gd-alloyed DSS (y = 1.750m)

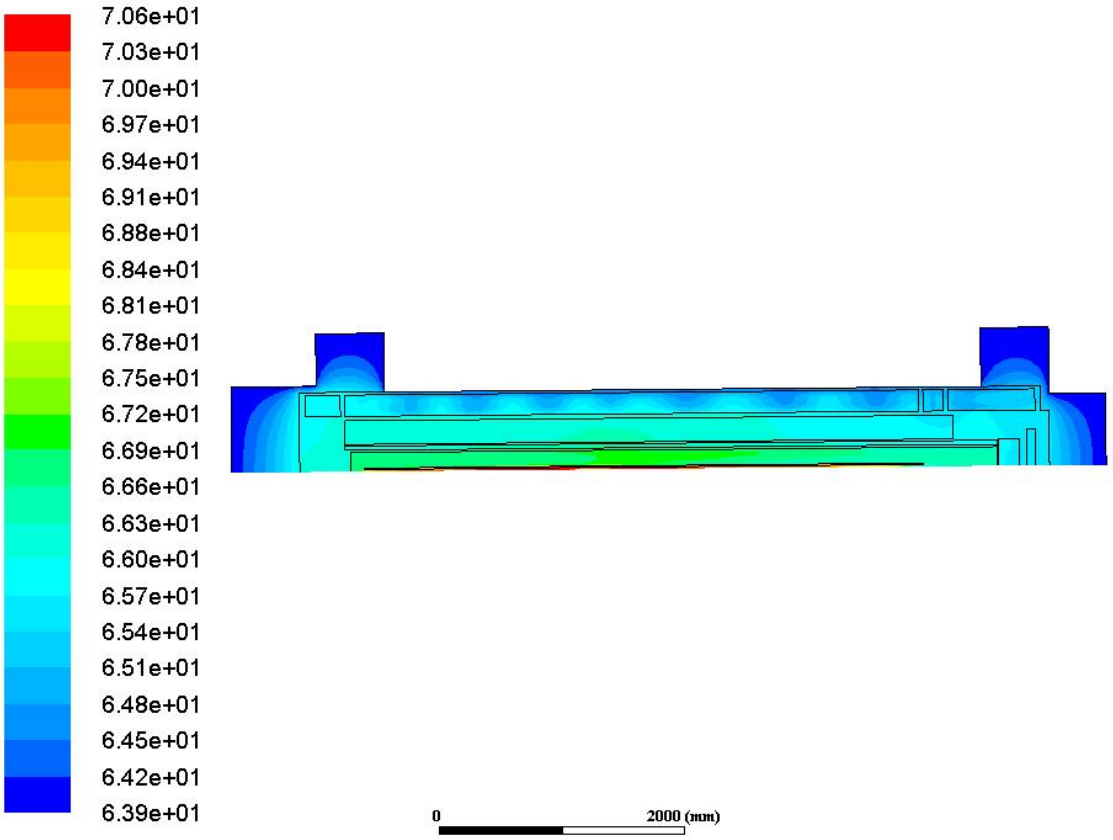

Figure 27. Temperature distribution of the KSC-1 which adopts Gd-alloyed DSS

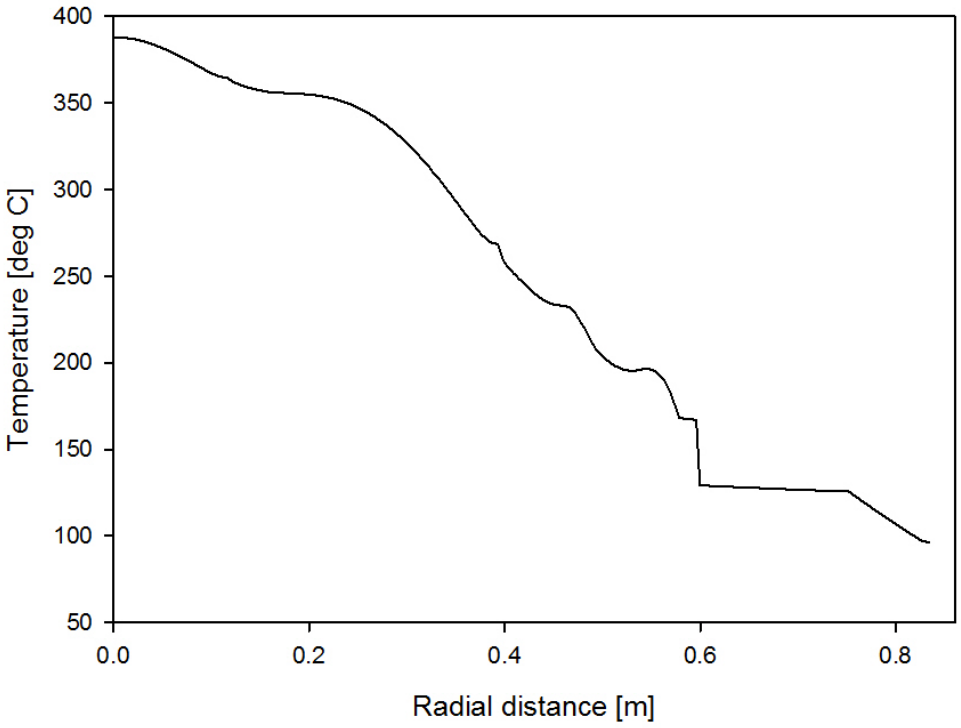

Figure 28. Radial temperature distribution of KORAD-21 which adopts the Gd-alloyed DSS (z =3.342m)

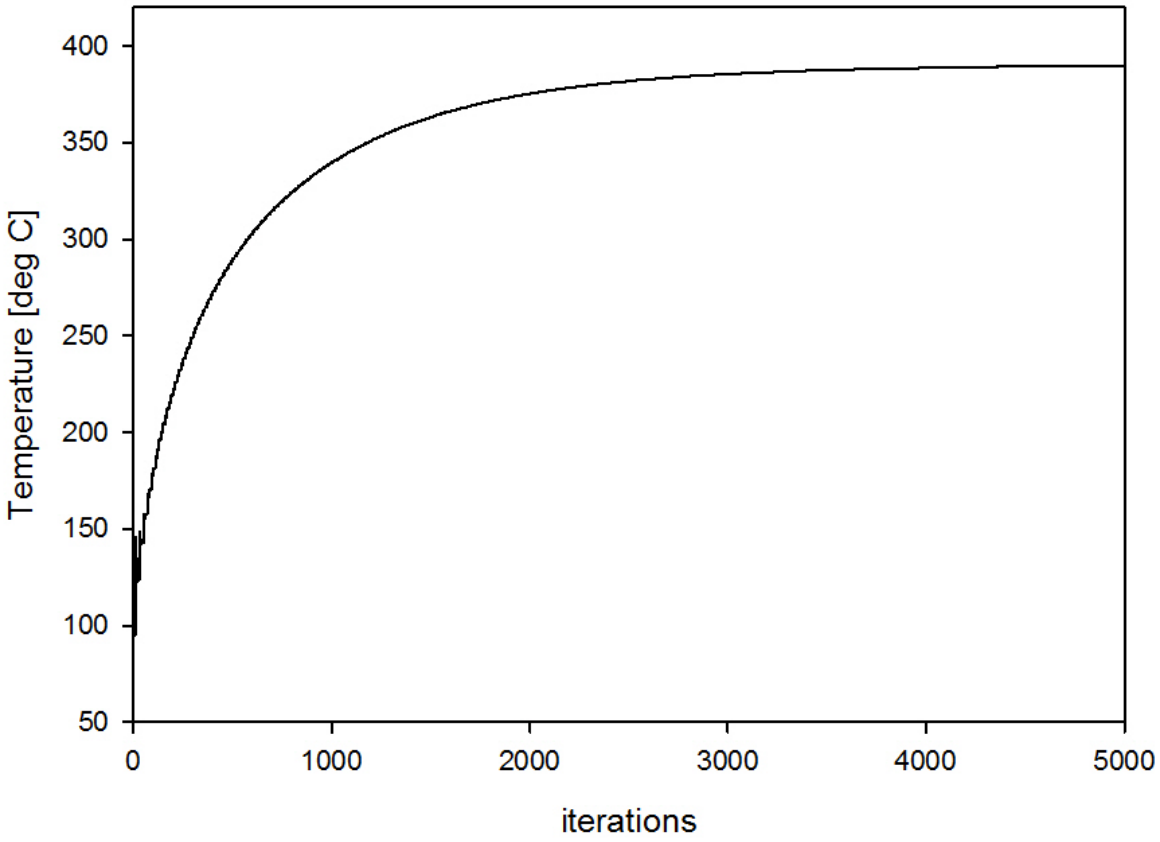

Figure 29. Convergence monitor of cladding temperature in the Gd-alloyed DSS case with 5.0mm basket wall thickness

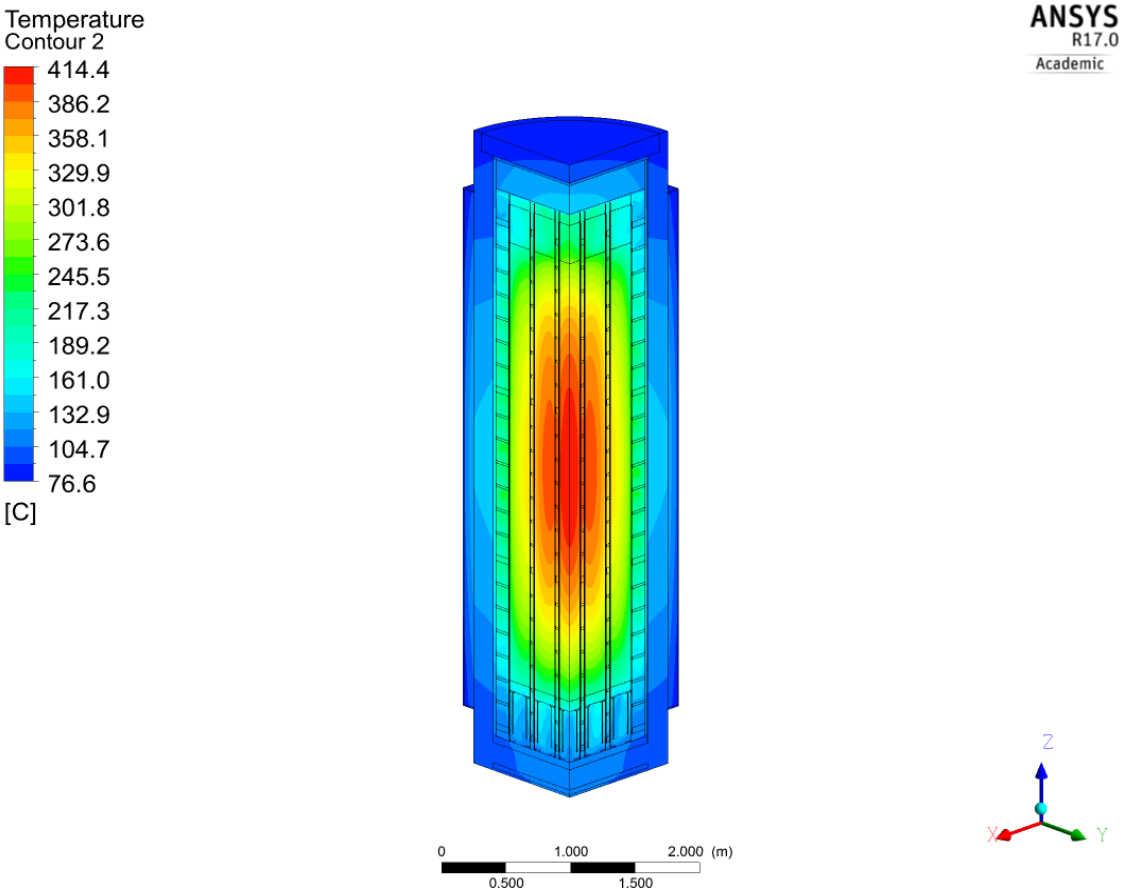

Figure 30. Temperature distribution of the KORAD-21 which adopts the Gd-alloyed DSS in 9.5mm basket wall thickness

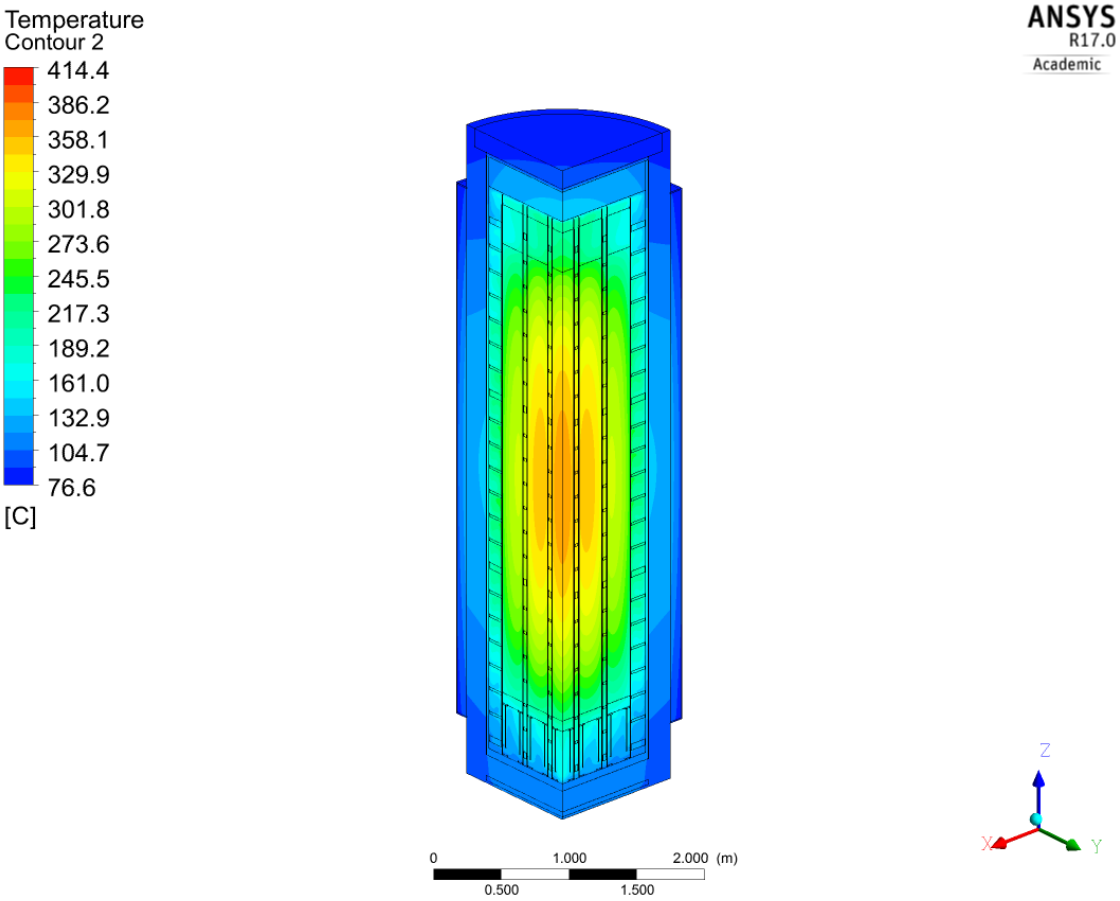

Figure 31. Temperature distribution of the BORAL case; temperature scale is same with the 9.5mm Gd-alloyed DSS case

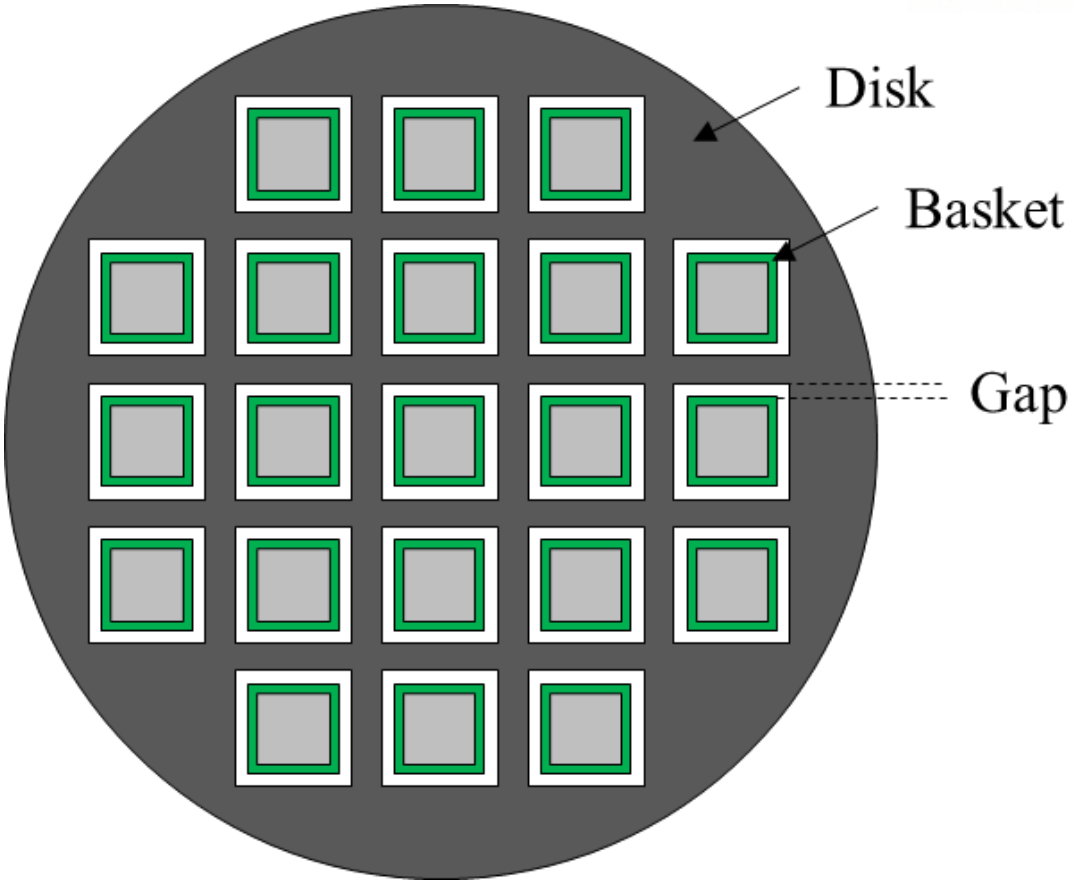

Figure 32. Gap between basket structures and disk square holes

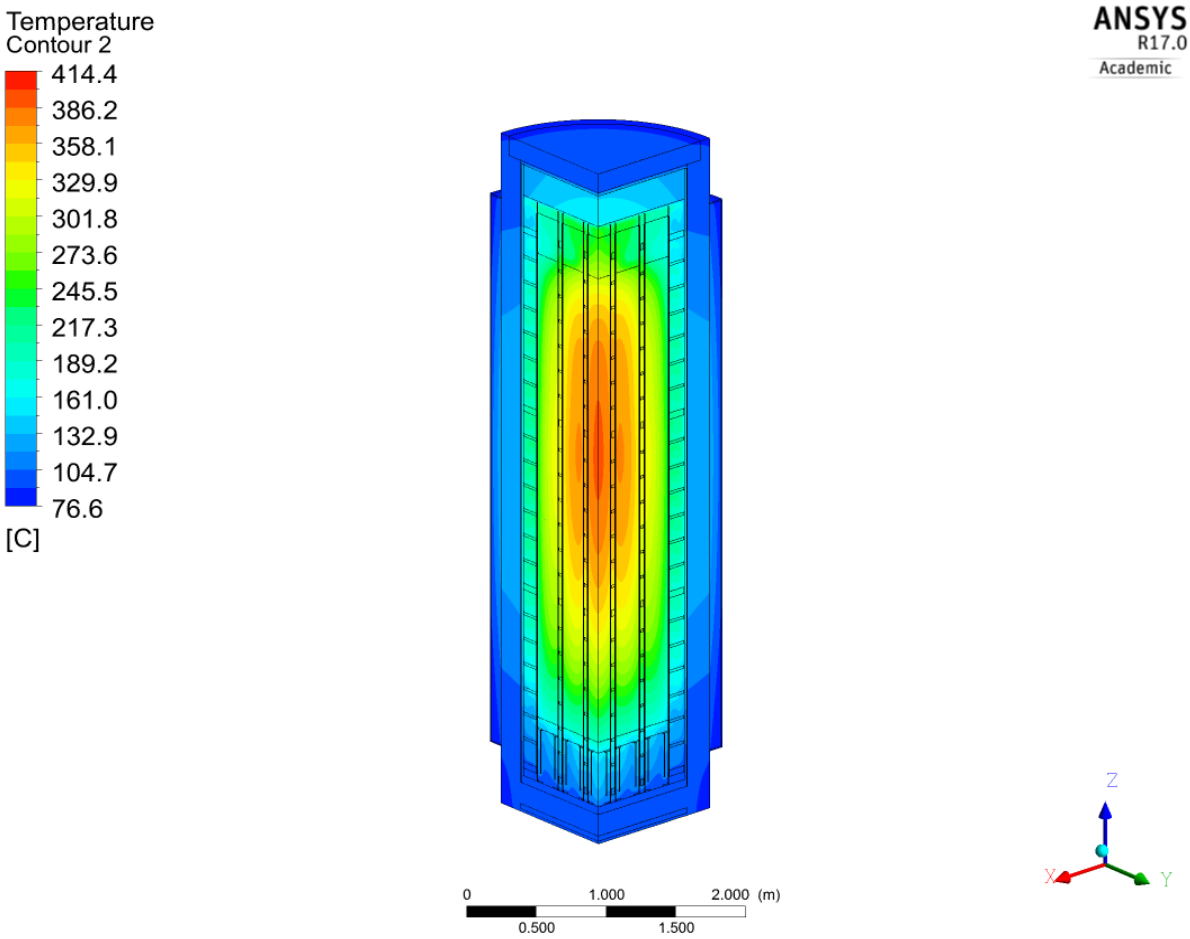

Figure 33. Temperature distribution of the Gd-alloyed DSS case with 5.0mm basket wall thickness; temperature scale is same with the 9.5mm Gd-alloyed DSS case

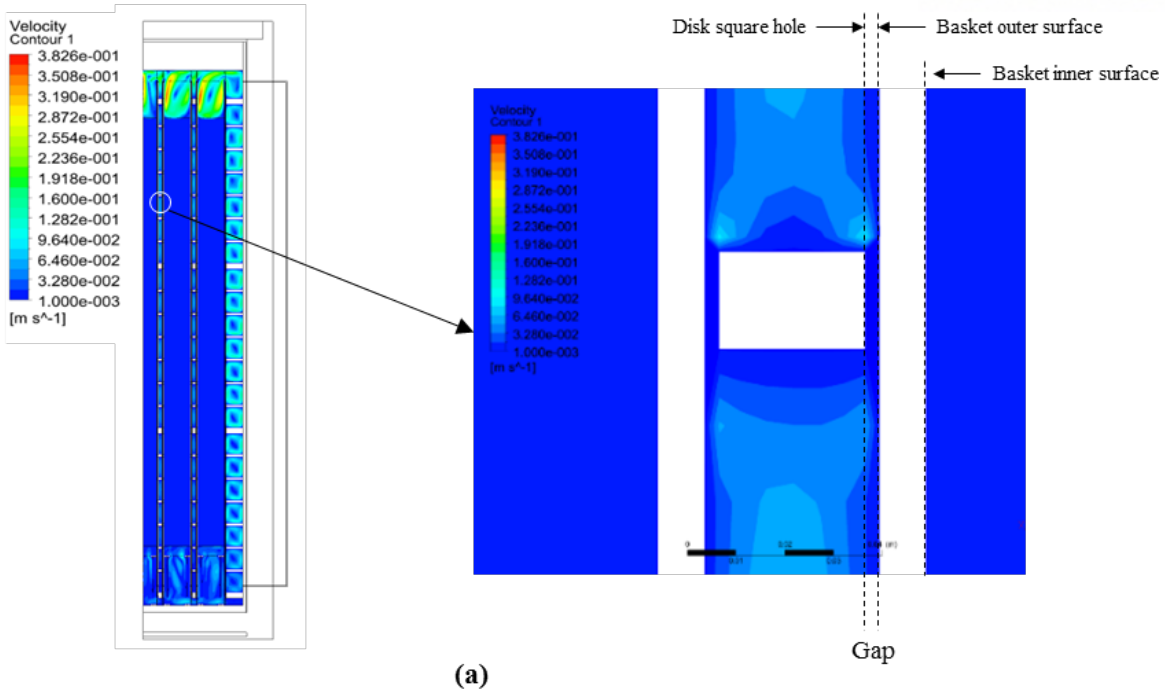

Figure 34. Velocity distribution of KORAD-21 cask with Gd-alloyed DSS; (a) the 9.5mm basket wall thickness case (b) the 5.0mm basket wall thickness case

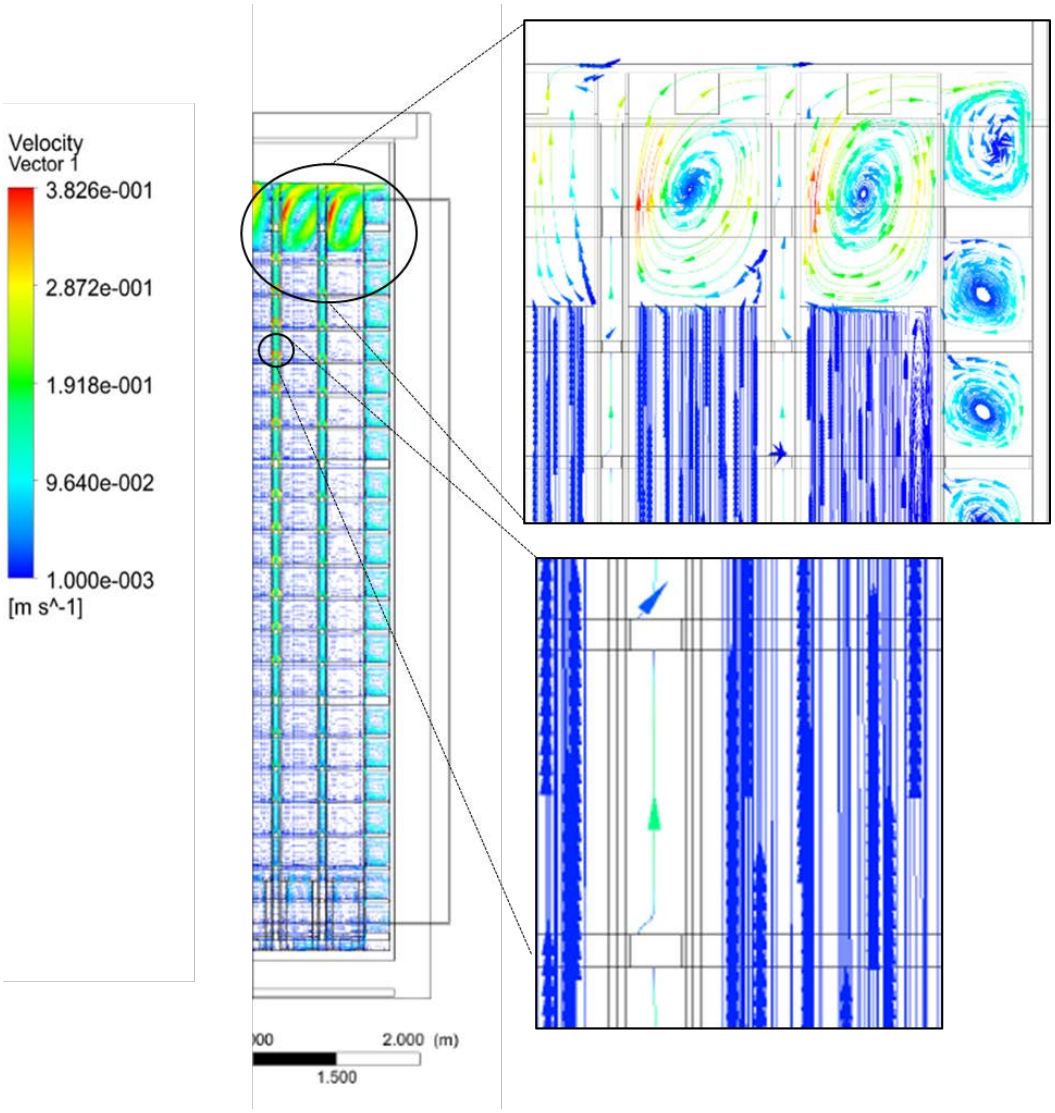

Figure 35. Velocity streamline of the 5mm basket wall thickness case with Gd-alloyed DSS

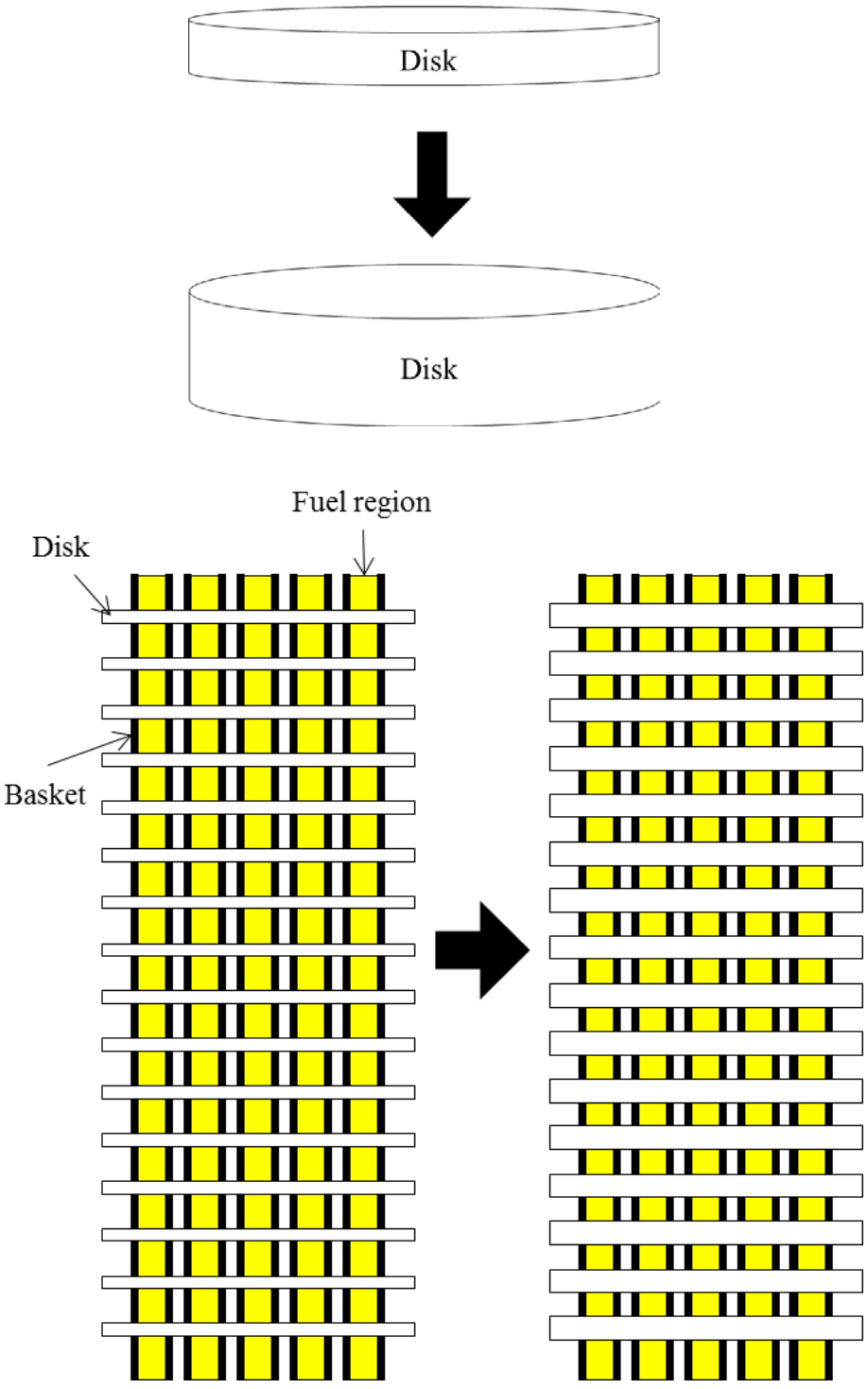

Figure 36. Shell conduction model of disk

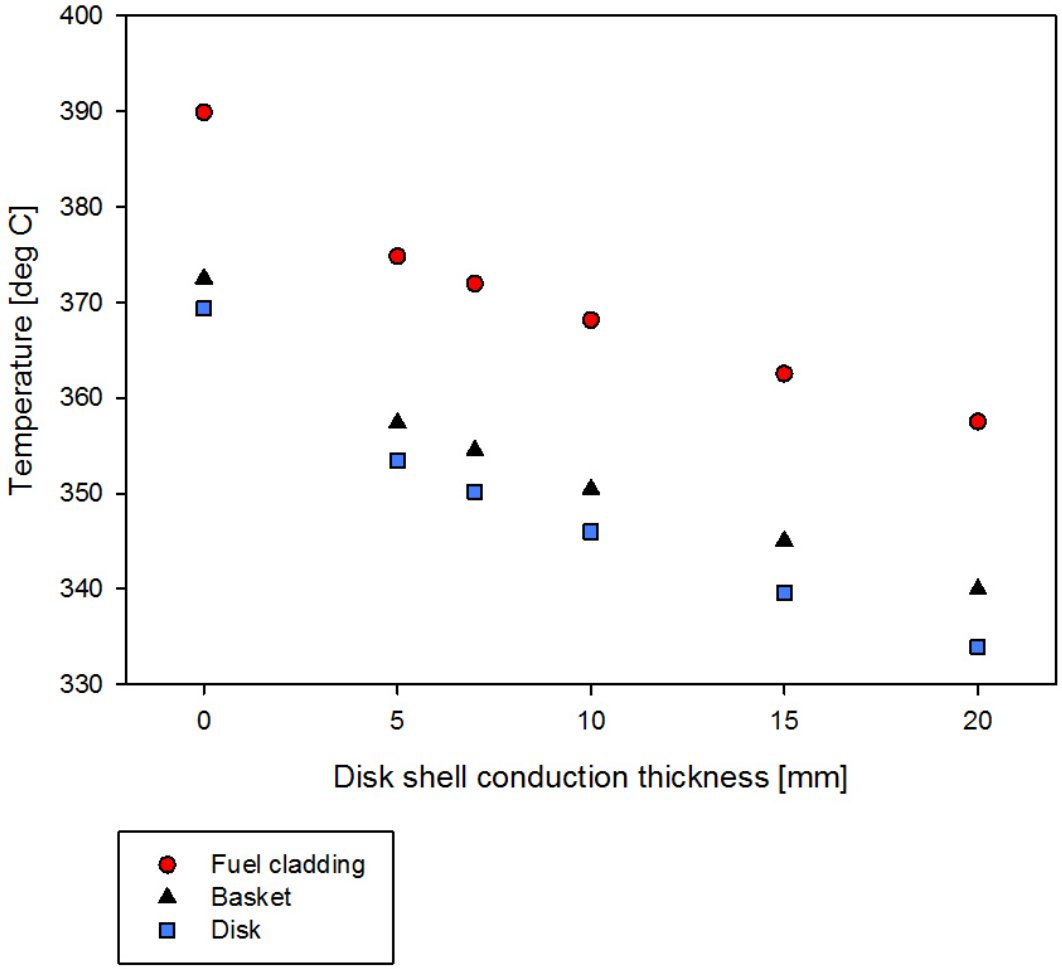

Figure 37. Maximum temperatures of fuel cladding, basket and disk as disk thickness increase

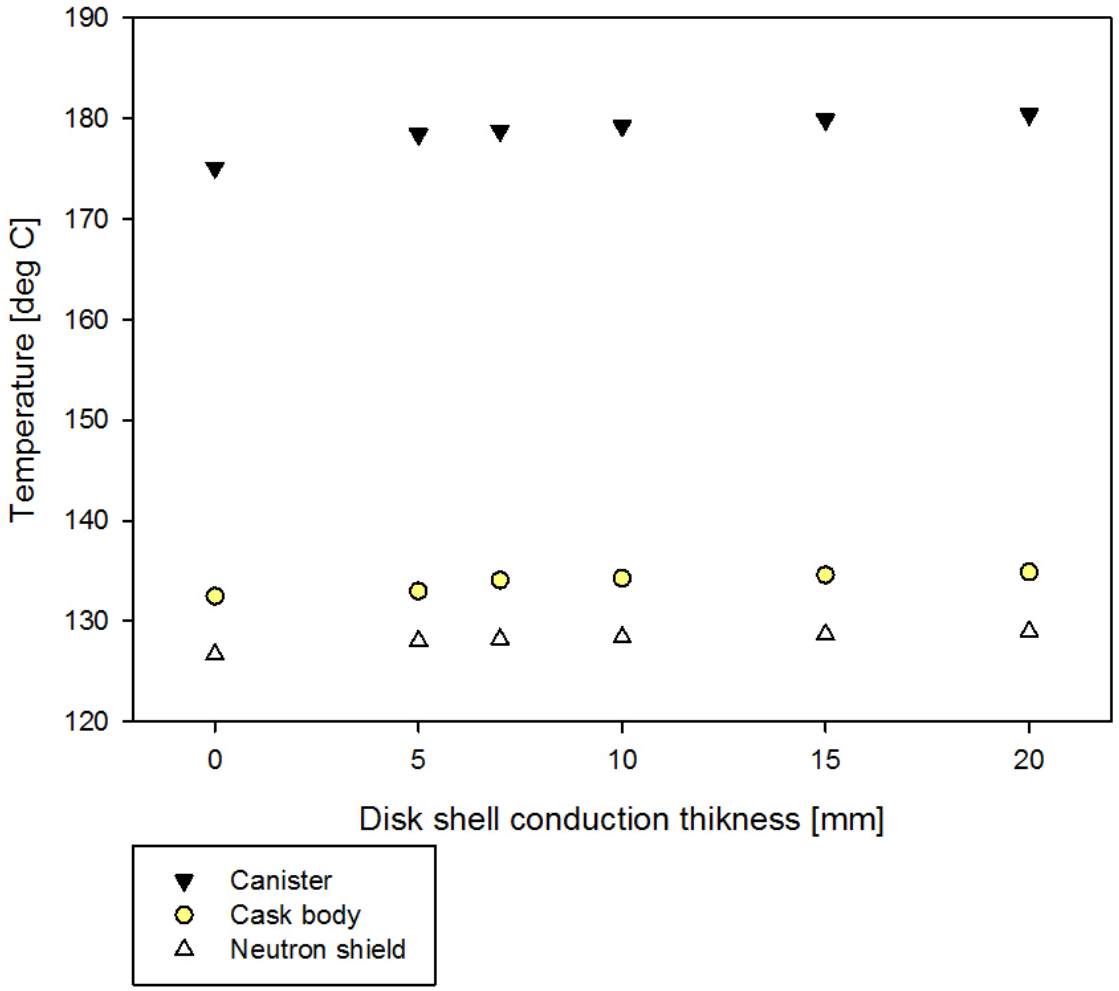

Figure 38. Maximum temperatures of canister, cask body and neutron shield as increase of disk thickness

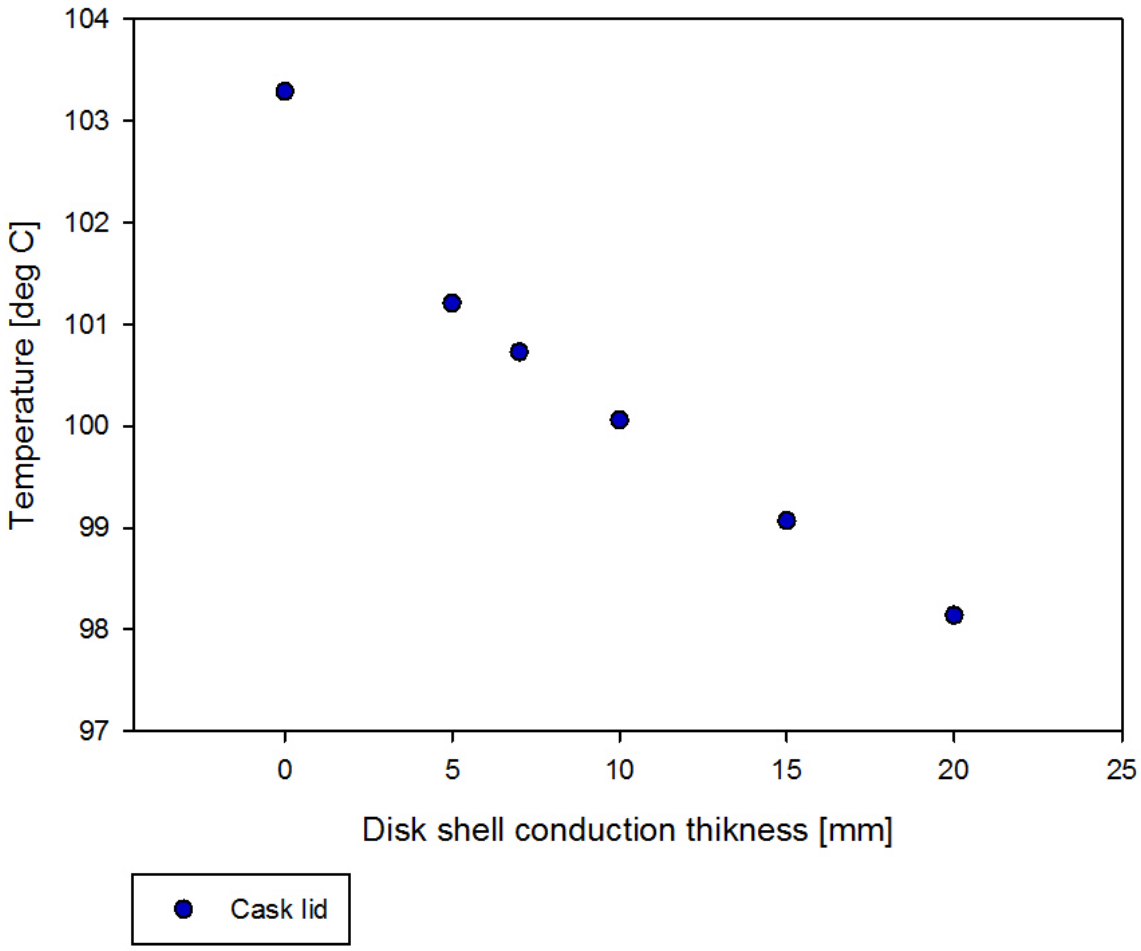

Figure 39. Maximum temperatures of cask lid as increase of disk thickness

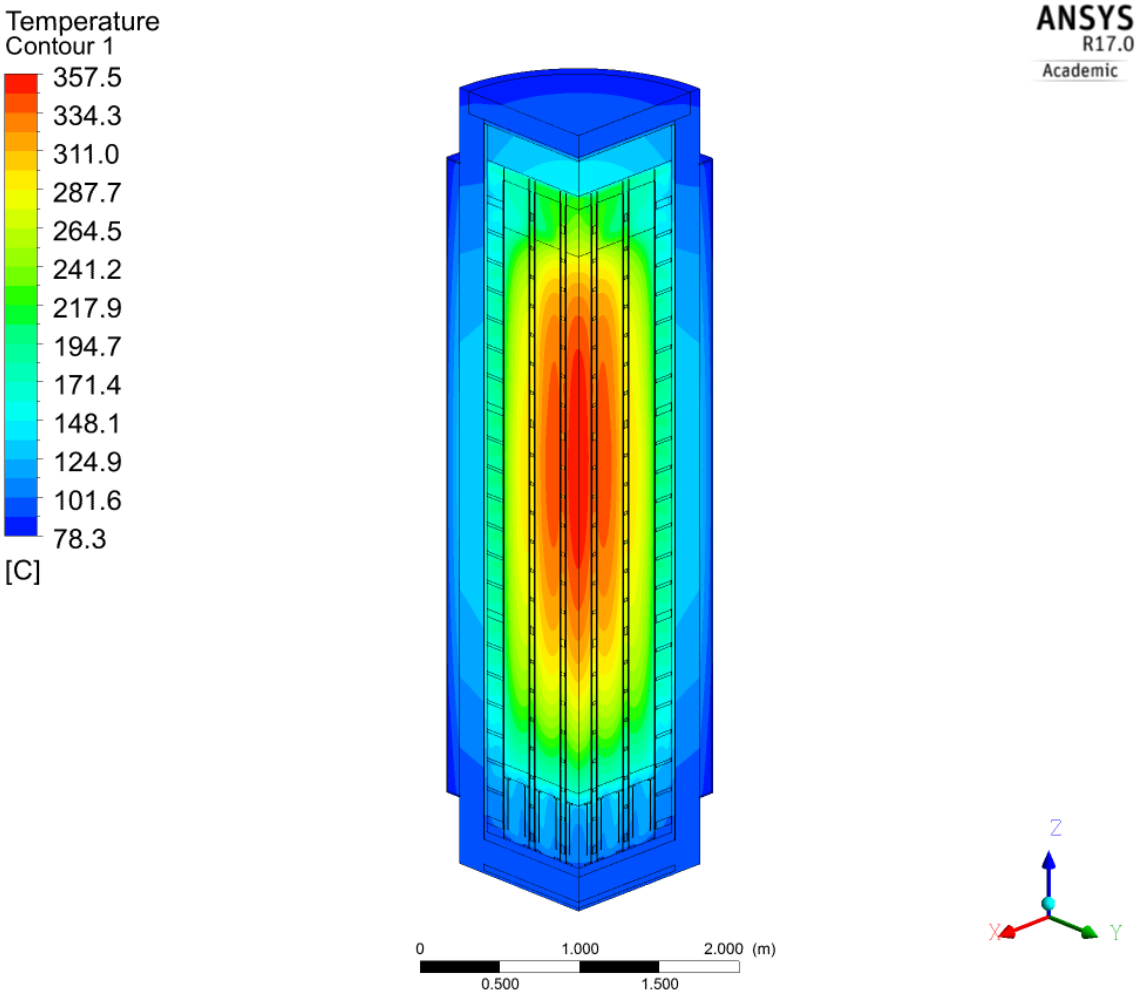

Figure 40. Temperature distribution of UNIST design cask

Table 1. Thermal neutron absorption cross-section of boron and gadolinium [4]

Nuclides	Thermal neutron absorption cross section, barn	Relative abundance, at%
B-10	3,840	19.9
B-11	0.005	80.1
Gd-152	1,400	0.20
Gd-154	290	2.18
Gd-155	62,540	14.80
Gd-156	12	20.47
Gd-157	255,000	15.65
Gd-158	7	24.84
Gd-160	1.8	21.86

Table 2. Materials of KSC-1 cask

Materials	Components
UO2 & Zircaloy	Fuel region
Water	Fuel cavity Inner cavity Upper neutron shield
Stainless steel	Basket Cask body Inner shell Intermediate shell Outer shell
Lead	Lead shield Inner closure shield
Air	Closure cavity Upper expansion cavity Lower air cavity
Ethylene-Glycol & Water	Neutron shield
Balsa wood	Impact limiter

Table 3. Materials of KORAD-21 cask

Materials	Components
Stainless steel; SA-240 304	Basket Disk Rod support Fuel support Cask body outer shell
Stainless steel; SA-240 316L	Canister Canister lid
BORAL	Neutron absorber
Resin; NS-4-FR;	Neutron shield
Carbon steel; SA-350 LF3	Cask body
SA-180 F6NM	Cask lid
Helium	Cavity
SA-516 70	Heat transfer fin

Table 4. Specifications of test specimens for thermal property measurement

Samples		Size	Sample ID
Duplex stainless steel	Alloy casting	D:6mm T:0.8mm (for DSC) D:10mm & T:2mm (for LFA)	DSS_00Gd_C
	Hot rolling	D:6mm T:0.8mm (for DSC) D:10mm & T:2mm (for LFA)	DSS_00Gd_H
0.6wt.% Gd-alloyed Duplex stainless steel	Alloy casting	D:6mm T:0.8mm (for DSC) D:10mm & T:2mm (for LFA)	DSS_06Gd_C
	Hot rolling	D:6mm T:0.8mm (for DSC) D:10mm & T:2mm (for LFA)	DSS_06Gd_H
0.7wt.% Gd-alloyed Duplex stainless steel	Alloy casting	D:6mm T:0.8mm (for DSC) D:10mm & T:2mm (for LFA)	DSS_07Gd_C
	Hot rolling	D:6mm T:0.8mm (for DSC) D:10mm & T:2mm ((for LFA)	DSS_07Gd_H

Table 5. Density measurement

Sample ID	Thickness[mm]						Mass[g]			Density
	1	2	3	4	5	Avg	Dry	Susp.	Sat.	g/cc
DSS_00Gd_C	1.996	1.997	1.995	1.995	1.996	1.996	1.2347	1.0778	1.2347	7.8552
DSS_00Gd_H	2.043	2.043	2.041	2.042	2.041	2.042	1.2649	1.1043	1.2649	7.8619
DSS_06Gd_C	1.997	1.998	1.997	1.999	1.996	1.997	1.2361	1.0791	1.2361	7.8591
DSS_06Gd_H	2.032	2.032	2.031	2.032	2.032	2.032	1.2579	1.0984	1.258	7.8674
DSS_07Gd_C	2.001	2.001	1.999	2.001	2.003	2.001	1.2355	1.0788	1.2356	7.8653
DSS_07Gd_H	2.031	2.032	2.031	2.030	2.030	2.031	1.2603	1.1006	1.2604	7.8725

Table 6. Specific heat measurement

Sample ID	Specific heat [J/gK]				
	50℃	100℃	200℃	300℃	400℃
DSS_00Gd_C	0.492	0.505	0.524	0.538	0.553
DSS_00Gd_H	0.476	0.489	0.507	0.519	0.536
DSS_06Gd_C	0.487	0.505	0.525	0.536	0.550
DSS_06Gd_H	0.483	0.500	0.514	0.526	0.537
DSS_07Gd_C	0.476	0.489	0.509	0.515	0.526
DSS_07Gd_H	0.494	0.503	0.520	0.527	0.529

Table 7. Coefficients for Cowan corrections [33]

Coefficients	5 Half-times	10 Half-times
a	-0.1037162	-0.054825246
b	1.239040	0.16697761
c	-3.974433	-0.28603437
d	6.888738	0.28356337
e	-6.804883	-0.13403286
f	3.856663	0.02477586
g	-1.167799	0
h	0.1465332	0

Table 8. Thermal diffusivity measurement

Sample ID	Thermal diffusivity [mm^2/s]				
	50℃	100℃	200℃	300℃	400℃
DSS_00Gd_C	2.925	3.261	3.594	3.741	3.910
DSS_00Gd_H	2.973	3.229	3.621	3.744	3.774
DSS_06Gd_C	2.868	3.109	3.375	3.566	3.714
DSS_06Gd_H	3.027	3.231	3.839	3.959	4.181
DSS_07Gd_C	2.988	3.138	3.597	3.788	3.907
DSS_07Gd_H	2.908	3.281	3.533	3.707	3.727

Table 9. Thermal conductivity of Gd-alloyed duplex stainless steel

Sample ID	Thermal conductivity[W/mK]				
	50℃	100℃	200℃	300℃	400℃
DSS_00Gd_C	11.301	12.947	14.792	15.818	16.999
DSS_00Gd_H	11.124	12.406	14.430	15.277	15.917
DSS_06Gd_C	10.989	12.339	13.927	15.011	16.044
DSS_06Gd_H	11.512	12.700	15.516	16.399	17.680
DSS_07Gd_C	11.184	12.079	14.398	15.347	16.157
DSS_07Gd_H	11.310	13.003	14.467	15.391	15.509

Table 10. Solar radiation on KSC-1 cask surface [10 CFR 71]

Surfaces	Solar radiation[W/m^2]
Curved surface	400
Surfaces of horizontal installation	800
Surfaces of vertical installation	200
Bottom surface	none

Table 11. Solar radiation on KORAD-21 cask surface

Surface type	Solar radiation[W/m^2]	24-hour averaged solar radiation[W/m^2]
Curved surface	400	194
Surfaces of horizontal installation	800	388
Surfaces of vertical installation	200	97
Bottom surface	None	none

Table 12. Temperature difference calculation of the KSC-1 cask; reference case

Components	SAR KSC-1	Calculation results	Temperature differences, θ
Fuel rod surface	71 ℃	70.6 ℃	-1.4 %
Basket	67 ℃	66.8 ℃	-0.8 %
Inner cavity water	71 ℃	70.5 ℃	-1.4 %
Lead	67 ℃	66.3 ℃	-2.5 %
Ethylene-glycol mix	67 ℃	66.1 ℃	-3.0 %
Outer surface	66 ℃	65.1 ℃	-3.4 %
Ambient temperature	38 ℃	38.0 ℃	-

Table 13. Temperature difference calculation of the KORAD-21 cask with BORAL; reference case

Components	SAR KORAD-21	Calculation results	Temperature differences
Fuel cladding	361 ℃	369.6 ℃	2.5 %
Basket	355 ℃	351.0 ℃	-1.2 %
Disk	349 ℃	346.0 ℃	-0.9 %
Canister	174 ℃	177.2 ℃	2.1 %
Cask body	139 ℃	134.8 ℃	-3.6 %
Side shield	132 ℃	128.9 ℃	-2.9 %
Cask lid	95 ℃	94.9 ℃	-0.2 %
Ambient temperature	22 ℃	22 ℃	-

Table 14. Maximum temperature of KSC-1 which adopts Gd-alloyed DSS

Components	Calculation results	Allowable temperature
Fuel rod surface	70.6 ℃	Max. 400 ℃
Basket	66.9 ℃	Max. 427 ℃
Inner cavity water	70.5 ℃	Max. 427 ℃
Lead	66.4 ℃	Max. 327 ℃
Ethylene-glycol mix	66.3 ℃	Min. -40 ℃
Outer surface	65.2 ℃	
Ambient temperature	38 ℃	

Table 15. Maximum temperatures of the 9.5mm basket wall thickness with Gd-alloyed DSS

Components	Calculation results	Allowable temperature
Fuel cladding	414.4 ℃	Max. 400 ℃
Basket	396.5 ℃	Max. 427 ℃
Disk	391.2 ℃	Max. 427 ℃
Canister	182.2 ℃	Max. 427 ℃
Cask body	137.7 ℃	Max. 371 ℃
Neutron shield	131.6 ℃	Max. 399 ℃
Cask lid	94.6 ℃	-40~340 ℃

Table 16. Maximum temperatures of the 5mm basket wall thickness with Gd-alloyed DSS

Components	Calculation results	Allowable temperature
Fuel cladding	389.9 ℃	Max. 400 ℃
Basket	372.5 ℃	Max. 427 ℃
Disk	369.4 ℃	Max. 427 ℃
Canister	175.1 ℃	Max. 427 ℃
Cask body	132.5 ℃	Max. 371 ℃
Neutron shield	126.7 ℃	Max. 399 ℃
Cask lid	103.3 ℃	-40~340 ℃

Table 17. Maximum temperatures as an increase of disk thickness

Components	Disk thickness					
	20 mm	30 mm	34 mm	40 mm	50 mm	60 mm
Fuel cladding	389.9 ℃	374.8 ℃	372.0 ℃	368.2 ℃	362.6 ℃	357.5 ℃
Basket	372.5 ℃	357.4 ℃	354.5 ℃	350.4 ℃	345.0 ℃	340.0 ℃
Disk	369.4 ℃	353.4 ℃	350.2 ℃	346.0 ℃	339.6 ℃	333.9 ℃
Canister	175.1 ℃	178.4 ℃	178.8 ℃	179.3 ℃	179.9 ℃	180.4 ℃
Cask body	132.5 ℃	133.9 ℃	134.1 ℃	134.3 ℃	134.6 ℃	134.9 ℃
Neutron shield	126.7 ℃	128.1 ℃	128.2 ℃	128.4 ℃	128.7 ℃	129.0 ℃
Cask lid	103.3 ℃	101.2 ℃	100.7 ℃	100.1 ℃	99.1 ℃	98.1 ℃

Table 18. Calculation results of UNIST design cask

Components	Calculation results of UNIST design cask	Allowable temperature
Fuel cladding	357.5 ℃	Max. 400 ℃
Basket	340.0 ℃	Max. 427 ℃
Disk	333.9 ℃	Max. 427 ℃
Canister	180.4 ℃	Max. 427 ℃
Cask body	134.9 ℃	Max. 371 ℃
Neutron shield	129.0 ℃	Max. 399 ℃
Cask lid	98.1 ℃	-40~340 ℃

V. Reference

[1] Juseong Kim., Hakkyu Yoon., Donghak Kook., & Yongsoo Kim. (2013). *A Study on the Initial Characteristics of Domestic Spent Nuclear Fuels for Long Term Dry Storage.* Nuclear Engineering and Technology, vol. 45, p. 377-384.

[2] Jonathan, B.W. (2015). *Evaluation of Aluminum-Boron Carbide Neutron Absorbing Materials for Interim Storage of Used Nuclear Fuel*, University of Michigan.

[3] Joe T. Carter, Seve. Maheras., & Robert Jones, (2016). *Containers for Commercial Spent Nuclear Fuel*, U.S. Department of Energy.

[4] EPRI (2009), *Handbook of Neutron Absorber Materials for Spent Nuclear Fuel Transportation and Storage Applications(2005 ed.).* EPRI Technical Report, No.1019110, Palo Alto.

[5] Feife Zhang, Gang.Yu., Chenyang Lu, Xu Wang, & Lumin Wang (2013). *Distribution of Helium Bubbles in Al/B4C MMC Irradiated with 400keV He+ Ions*. *Microscopy Society of America.*

[6] EPRI (2004). *BORAL™ Behavior Under Simulated Cask Vacuum Drying Conditions (Part 2 Test Results),* EPRI Technical Report, No.1009696, Palo Alto.

[7] U.S. NRC (1979). *Nuclear Regulatory Commission Issuances: Opinions and Decisions of the Nuclear Regulatory Commission with Selected Orders*. vol. 9.

[8] Jack E. Rosenthal Memorandum.to Carl J.Paperiello (2004), *Results of Initial Screening of Generic Issue 196, "BORAL Degradation"*.

[9] Mi Jin Kim., Hee-Jae Lee., & Dong-Seong Sohn (2016). *The Effectiveness of Gd Contents of Fuel Basket Wall in UNF Shipping & Storage Cask*, Waste Management, Pheonix, Arizona, USA.

[10] Mi Jin Kim., Hee-Jae Lee., & Dong-Seong Sohn (2017). *The Gd based Neutron Absorber for Spent Fuel Storage and Transport Cask*, Waste Management. Pheonix, Arizona, USA.

[11] Y. Choi., B. M. Moon., & D. S. Sohn (2013). *Fabrication of Gd Containing Duplex Stainless Steel Sheet for Neutron Absorbing Structural Materials.* Nuclear Engineering and Technology, vol. 5, p. 689-694.

[12] 10 CFR 72 (2014). *Licensing Requirements for the Independent Storage of Spent Nuclear Fuel and High Level Radioactive Waste and Reactor-Related Greater than Class C waste*.

[13] 10 CFR 71 (2014). *Packagin and Transportation of Radioactive Material*.

[14] U.S.NRC (2000). *Standard Review Plan for Spent Fuel Dry Storage Facilities, NUREG-1567,* Washington, DC.

[15] U.S.NRC (2009). *Standard Review Plan for Dry Cask Storage Systems, NUREG-1536,* Washington, DC.

[16] U.S. NRC (2003). *SFST-ISG-11, Revision 3, 'Cladding Considerations for the Transportation and Storage of Spent Fuel'*.

[17] Nobuyuki Yamada., Ryuichi Horita., Katsunori Kusunok.i, Akio O-iwa., & Ryoji Asano (2004). *Thermal Behavior of Neutron Shielding Material, NS-4-FR, under Long Term Storage Conditions*, 14th International Symposium on the Packaging and Transportation of Radioactive Materials(*PATRAM 2004)*, September 20-24, Berlin, Germany.

[18] Wooton, R.O., & H.M. Epstein (1963). *Heat Transfer from a Parallel-Rod Fuel Assembly in a Shipping Container*, Battelle Memorial Institute.

[19] Bahney, R.H., & Lotz, T.L.(1996). *Spent Nuclear Fuel Effective Thermal Conductivity Report*, US Department of Energy.

[20] Manteufel, R.D., & Todreas, N.E.(1994). *Effective Thermal Conductivity and Edge Conductance Model for a Spent Fuel Assembly.* Nuclear Tecnology, vol. 405: p. 421-440.

[21] Gomez, P.E.A., & Greiner, M., *Simulation of Heat Transfer within the Fuel Assembly/ backfill Gas Region of Transport Packages, ASME 2005 Pressure Vessels and Piping Conference*, Danver, Colorado, USA.

[22] Hyungjin Kim., Oh Joon Kwon., Gyeong-Uk Kang., & Dong-Gyu Lee(2014). *Comparisons of Prediction Methods for Peak Cladding Temperature and Effective Thermal Conductivity in Spent Fuel Assemblies of Trasportation/Storage Casks.* Annals of Nuclear Energy, vol. **71**: p. 427-435.

[23] HOLTEC Inc. *Safety Analysis Report for the HI-STAR 100 Cask System,* (*revision 10*), HI-951251.

[24] J.-C. Lee, D.-H.Kim., K.-S. Seo, B.-I.Choi, & H.-Y. Lee(2005). *Thermal Analysis of a Storage Cask for 24 Spent PWR Fuel Assemblies,* Packaging, Transport, Storage & Security of Radioactive Material, vol. **16**(1), p. 19-26

[25] Creer, J.M., Michener, T.E., McKinnon, M.A., Tanner, J.E., Gillbert, E.R., Dziadosz, D.A., Moore, E.V., Schoonen, D.H., & Jensen, M.F.(1987). *The TN-24P PWR Spent Fuel Storage Cask: Testing and Analysis,* EPRI-NP-5128, Palo Alto, California.

[26] J.C. Lee., W.S.Choi., K.S. Seo., & S.Y. Yoo.(2008) *Thermal-Fluid Flow Analysis and Demostration Test of a Spent Fuel Storage System,* Nuclear Engineering Design, vol. 238, p. 551-558.

[27] Hyoung-Mun Kwon., Jung-Nam Jang., Yong-Hwa Hwang., In-Chan Kwon., Duck-Kee Min., & Yong-Bum Chun.(2010). *Shielding and Criticality Safety Analysis of KSC-1 Cask for the High Burnup PWR Spent Fuels, Korean Nuclear Society, October 21-22,* Jeju, Korea.

[28] KAERI (2009). *후행핵연료주기 정책방안을 위한 기초연구 (최종보고서).*

[29] Frank P. Incropera, David P. Dewitt, Theodore L. Bergman, & Adrienne S. Lavine (2008), *Fundamentals of Heat and Mass Transfer(6th edition),* John Wiley & Sons.

[30] 유승환, 방경식, 이주찬 & 최우석 (2015), *단위바스켓 유동특성 평가,* Korean Radioactive Waste Society.

[31] Hee-Jae Lee., Mi Jin Kim., & Dong-Seong Sohn.(2016), *The Effective Thermal Conductivity of Spent Fuel Assemblies for Spent Fual Storage,* Korean Radioactive Waste Society.

[32] Höhne, Günther, Hemminger Wolfgang F., Flammersheim, & H.-J.(2003), *Differential Scanning Calorimetry*, Springer-Verlag Berlin Heidelberg.

[33] Cowan, R.D(1963). *Pulse Method of Measuring Thermal Diffusivity at High Temperature.* Journal of Applied Physics, vol. 34, p. 926-927.

[34] Phyllis M. Lovett, & Nail E. Todreas.(1991), *An Experiment to Simulate the Heat Transfer Properties of a Dry, Horizontal Spent Nuclear Fuel Assembly*. MITNE-294.

[35] KAERI (2015), *Safety Analysis Report of KSC-1(Revision 2)*.

[36] Holman, J.P. (2010), *Heat Trnasfer*, McGraw-Hill.

[37] (Chun-Hyung Cho, personal communication, June 3, 2015)

[38] ANSYS Inc.(2009), *ANSYS FLUENT 12.0 Theory Guide*.

[39] Luis E. Herranz, Jaime Penalva, & Francisco Feria(2015), *CFD analysis of a cask for spent fuel dry storage: Model fundamentals and sensitivity studies*, Annals of Nuclear Energy, vol. **76**, p. 54-62.